Second-order homogenization of boundary and transmission conditions for one-dimensional waves in periodic media

Rémi Cornaggia, Bojan B Guzina

Second-order homogenization of boundary and transmission conditions for one-dimensional waves in periodic media

R. Cornaggia[a,*], B. B. Guzina[b]

[a] *Aix Marseille Univ, CNRS, Centrale Marseille, LMA UMR 7031, Marseille, France*
[b] *Department of Civil, Environmental, and Geo-Engineering, University of Minnesota, Twin Cities*

Abstract

We consider the homogenized boundary and transmission conditions governing the mean-field approximations of 1D waves in finite periodic media within the framework of two-scale analysis. We establish the homogenization ansatz (up to the second order of approximation), for both types of problems, by obtaining the relevant boundary correctors and exposing the enriched boundary and transmission conditions as those of Robin type. Rigorous asymptotic analysis is performed for boundary conditions, while the applicability to transmission conditions is demonstrated via numerical simulations. Within this framework, we also propose an optimized second-order model of the homogenized wave equation for 1D periodic media, that follows more accurately the exact dispersion relationship and generally enhances the performance of second-order approximation. The proposed analysis is applied toward the long-wavelength approximation of waves in finite periodic bilaminates, subject to both boundary and transmission conditions. A set of numerical simulations is included to support the mathematical analysis and illustrate the effectiveness of the homogenization scheme.

Keywords: Homogenization; wave equation; effective boundary conditions; effective transmission conditions; boundary correctors

1. Introduction

To help the fundamental understanding of wave motion in periodic media, many asymptotic models cater for a homogenized description of the wave equation, usually valid over a specific range of frequencies. In particular, in the low-frequency limit (i.e. for small periodicity-lengthscale-to-wavelength ratio ε), the two-scale homogenization framework Bensoussan et al. (1978); Cioranescu and Donato (1999) is well established and enables asymptotic description of the incipient wave dispersion when pursued up to the second order Santosa and Symes (1991); Fish et al. (2002); Andrianov et al. (2008); Lamacz (2011); Wautier and Guzina (2015); Allaire et al. (2016). To understand the wave motion in *bounded* periodic domains (e.g. microstructured obstacles), however, it is necessary to complement the homogenized wave equation with commensurate boundary or transmission conditions, such that the homogenized solution of a relevant boundary value problem converges toward its limit (as $\varepsilon \to 0$) at the same rate as the homogenized field equation Cioranescu and Donato (1999); Vinoles (2016); Cakoni et al. (2016).

When tackling two- or three-dimensional wave problems, finding such boundary and transmission conditions is highly challenging due to the presence of rapidly oscillating *boundary layers* near lines or surfaces where the periodic structure terminates. Many existing works are dedicated to describing these layers in terms of the *boundary correctors* that must be included in the asymptotic analysis of boundary value problems Dumontet (1986); Moskow and Vogelius (1997); Allaire and Amar (1999); Gérard-Varet and Masmoudi (2012); Armstrong et al. (2017) and transmission problems Cakoni et al. (2016); Lin and Meng (2019); Cakoni et al. (2019). Recently, equivalent boundary and transmission conditions were developed for a wide variety of microstructured surfaces and interfaces Claeys and Delourme (2013); Marigo et al. (2017); Semin et al. (2018), but their applications in the context of multi-dimensional periodic composites are extremely limited to planar boundaries and interfaces, aligned with one of the principal directions of the lattice Vinoles (2016); Marigo and Maurel (2017); Maurel and Marigo (2018).

*Corresponding author.
Email addresses: cornaggia@lma.cnrs-mrs.fr (R. Cornaggia), guzin001@umn.edu (B. B. Guzina)

For one-dimensional (1D) problems, on the other hand, the domain boundaries and interfaces reduce to points and some key difficulties of the multi-dimensional analysis can be avoided. In this vein, we consider (both theoretically and numerically) 1D homogenized boundary and transmission conditions featuring the boundary correctors up to the second order of approximation, i.e. $O(\varepsilon^2)$. Beyond providing a reference solution for more involved 2D or 3D homogenized models, such simplified configurations are directly relevant to a number of engineering problems such as the low-frequency axial vibrations of periodic beams, acoustic propagation in waveguides, and wave motion in periodically-layered materials under the condition of normal incidence.

We begin by summarizing in Section 2 the key results of higher-order (two-scale) homogenization of the 1D wave equation in periodic media. In Section 3 we propose a set of enhanced, Robin-type homogenized boundary conditions – up to the second order of asymptotic approximation, we establish the underpinning convergence estimates, and we discuss the application of these results to transmission conditions. With the (second-order) homogenized field equation and boundary conditions at hand, in Section 4 we pursue the two-scale approximation of waves in a finite periodic bilaminate featuring both Dirichlet and Neumann boundary conditions. To maximize the fidelity of the asymptotic model, we further propose an optimized version of the second-order effective wave equation that makes use of the exact dispersion relationship. We next compute the exact and homogenized solutions for both (i) boundary value problem, and (ii) transmission problem featuring a periodic bilaminate. The results of numerical simulations that include dispersion diagrams, mean-field approximations, "full"-field approximations, and convergence studies are found to consistently support the mathematical analysis. For completeness, specifics of the homogenization ansatz for periodic bilaminate are provided in the appendices.

2. Second-order homogenization of the 1D wave equation

In what follows, we provide the relevant background on the two-scale homogenization of wave motion in periodic media. Our focus is on the 1D time-harmonic problem; we refer to Bensoussan et al. (1978); Cioranescu and Donato (1999) for general asymptotic analysis of periodic structures, and to Wautier and Guzina (2015) for analysis of the corresponding time-domain problem.

Consider the time-harmonic, longitudinal wave motion in a micro-structured elastic rod whose Young's modulus E_r and mass density ρ_r are ℓ-periodic. To cater for physical applications, we assume that

$$E_{\min} \leqslant E_r \leqslant E_{\max} \quad \text{and} \quad \rho_{\min} \leqslant \rho_r \leqslant \rho_{\max}, \tag{1}$$

where $E_{\min}, E_{\max}, \rho_{\min}$ and $\rho_{\max}$ are positive constants. We further assume that the wave motion occurs in a neighborhood of some *reference frequency* $\omega_\circ$, e.g. the central frequency of a narrow-band excitation signal in the time domain.

Remark 1. *Hereon, we render all quantities dimensionless by making reference to the dimensional basis*

$$E_\circ,\ \rho_\circ,\ \lambda_\circ := \frac{2\pi\sqrt{E_\circ/\rho_\circ}}{\omega_\circ}.$$

Unless stated otherwise, we select $E_\circ = E_{\min}$ and $\rho_\circ = \rho_{\max}$. In this setting, the unit cell of periodicity becomes

$$Y_\varepsilon = \{x \in \mathbb{R} : 0 < x < \varepsilon\},$$

where ε signifies the unit cell size-to-wavelength ratio

$$\varepsilon := \frac{\ell}{\lambda_\circ},$$

while the material properties are described in terms of ε-periodic functions

$$E(x) = E_\circ^{-1} E_r(\lambda_\circ x), \qquad \rho(x) = \rho_\circ^{-1} \rho_r(\lambda_\circ x).$$

In the time-harmonic regime with (dimensionless) frequency ω, the longitudinal displacement $u(x)$ in the rod accordingly satisfies the field equation

$$(E(x)u_{,x})_{,x} + \rho(x)\,\omega^2 u = 0, \tag{2}$$

where $f_{,x} = \partial f/\partial x$.

In pursuing the effective description of (2), we assume the *separation of scales* in that $\ell \ll \lambda_\circ$; accordingly we conduct the asymptotic analysis as $\varepsilon \to 0$. By the adopted normalization scheme, this limit corresponds to either: (i) the wave motion at fixed "center" frequency, $\omega_\circ$, in microstructures of decreasing characteristic lengthscale ℓ, or (ii) wave propagation through a fixed microstructure at diminishing "center" frequencies. For further reference, we note the implied lower bound on the (dimensionless) wavelength in the rod as

$$\omega = O(1) \quad \Longrightarrow \quad \lambda \geqslant \frac{2\pi}{\omega} \min_{x \in Y_\varepsilon} \sqrt{\frac{E}{\rho}} = \frac{2\pi}{\omega} = O(1). \tag{3}$$

2.1. Two-scale expansion

In the remainder of this work, we exploit the separation in order between the periodicity lengthscale, $|Y_\varepsilon| = \varepsilon$, and the $O(1)$ wavelengths (3) present in the problem. In the context of the two-scale analysis Bensoussan et al. (1978), this motivates the introduction of a "fast" spatial variable

$$y = \frac{x}{\varepsilon}. \tag{4}$$

On letting

$$Y = \{y \in \mathbb{R} : 0 < y < 1\},$$

the periodic coefficients in (2) can be conveniently described in terms of Y-periodic functions $\hat{E}$ and $\hat{\rho}$, while the axial displacement is sought as a function of both variables x and y, i.e.

$$E(x) = \hat{E}(y), \quad \rho(x) = \hat{\rho}(y) \quad \text{and} \quad u(x) = \hat{u}(x, y),$$

where $\hat{u}$ is Y-periodic in the second argument. In this setting, we also introduce the germane differential and averaging operators

$$\frac{\mathrm{d}}{\mathrm{d}x} = \frac{\partial}{\partial x} + \varepsilon^{-1} \frac{\partial}{\partial y} \quad \text{and} \quad \langle f \rangle = \int_0^1 f(y) \mathrm{d}y. \tag{5}$$

On substituting (4)–(5) into the time-harmonic wave equation (2), we obtain

$$\varepsilon^{-2} (\hat{E}\hat{u}_{,y})_{,y} + \varepsilon^{-1} \big[(\hat{E}\hat{u}_{,x})_{,y} + (\hat{E}\hat{u}_{,y})_{,x} \big] + \hat{E}\hat{u}_{,xx} + \hat{\rho}\,\omega^2 \hat{u} = 0. \tag{6}$$

The displacement field $\hat{u}$ is then sought as a formal series in ε, and we denote by $\hat{u}^{(p)}$ the restriction of this series to the first $p+1$ terms; in other words, we write

$$\hat{u}(x, y) = \sum_{j \geqslant 0} \varepsilon^j u_j(x, y) \quad \text{and} \quad \hat{u}^{(p)}(x) = \sum_{j=0}^{p} \varepsilon^j u_j(x, y). \tag{7}$$

Inserting (7) into (6) leads to a cascade of partial differential equations for u_j $(j = 0, 1, 2, \ldots)$. As examined in Fish et al. (2002); Andrianov et al. (2008); Lamacz (2011); Wautier and Guzina (2015), solving these equations yields a sequence of separated-variable solutions

$$\begin{aligned}
u_0(x, y) &= U_0(x), \\
u_1(x, y) &= U_1(x) + U_{0,x}(x) P_1(y), \\
u_2(x, y) &= U_2(x) + U_{1,x}(x) P_1(y) + U_{0,xx}(x) P_2(y), \\
u_3(x, y) &= U_3(x) + U_{2,x}(x) P_1(y) + U_{1,xx}(x) P_2(y) + U_{0,xxx}(x) P_3(y),
\end{aligned} \tag{8}$$

expressed in terms of the *mean fields*

$$U_j(x) = \langle u_j(x, \cdot) \rangle,$$

and the so-called *cell functions* $P_j(y)$ which are described next.

2.2. Cell functions and homogenized coefficients

As shown in the two-scale studies (e.g. Wautier and Guzina, 2015) of the 1D wave equation, the cell functions in (8) satisfy the respective *unit cell problems*

$$\left.\begin{array}{l} [\hat{E}(1+P_{1,y})]_{,y} = 0 \quad \text{in } Y \\ P_1 \ \text{ and } \ \hat{E}(1+P_{1,y}) \quad \text{are } Y\text{-periodic} \\ \langle P_1 \rangle = 0 \end{array}\right\}, \tag{9}$$

$$\left.\begin{array}{l} [\hat{E}(P_1+P_{2,y})]_{,y} = \mathcal{E}_0 \frac{\hat{\rho}}{\varrho_0} - \hat{E}(1+P_{1,y}) \quad \text{in } Y \\ P_2 \ \text{ and } \ \hat{E}(P_1+P_{2,y}) \quad \text{are } Y\text{-periodic} \\ \langle P_2 \rangle = 0 \end{array}\right\}, \tag{10}$$

and

$$\left.\begin{array}{l} [\hat{E}(P_2+P_{3,y})]_{,y} = \mathcal{E}_0 \frac{\hat{\rho}}{\varrho_0} P_1 - \hat{E}(P_1+P_{2,y}) \quad \text{in } Y \\ P_3 \ \text{ and } \ \hat{E}(P_2+P_{3,y}) \quad \text{are } Y\text{-periodic} \\ \langle P_3 \rangle = 0 \end{array}\right\}. \tag{11}$$

On letting $P_0 := 1$, the effective Young's modulus $\mathcal{E}_0$ and effective mass density ϱ_0 appearing in (10)–(11), together with their higher-order counterparts $\mathcal{E}_j$ and ϱ_j, $j \geqslant 1$ (to appear later), are given by

$$\mathcal{E}_j = \big\langle \hat{E}\big(P_j + P_{j+1,y}\big)\big\rangle \quad \text{and} \quad \varrho_j = \langle \hat{\rho} P_j \rangle, \quad j = 0, 1, 2 \ldots \tag{12}$$

From (12) we observe that: (i) the leading-order effective density ϱ_0 is given by the mean of $\hat{\rho}$ (this holds for any dimension of the problem), and (ii) $\mathcal{E}_0$ recovers the classical homogenization result for one-dimensional problems, namely

$$\mathcal{E}_0 = \big\langle \hat{E}^{-1} \big\rangle^{-1}.$$

We next assert a useful property, which also holds without any further assumptions on $\hat{E}$ and $\hat{\rho}$.

Lemma 1. *The effective coefficients $\mathcal{E}_0, \varrho_0, \mathcal{E}_1$ and ϱ_1 satisfy the identity*

$$\mathcal{E}_1 \ = \ \mathcal{E}_0 \frac{\varrho_1}{\varrho_0}. \tag{13}$$

Proof. Although the claim of this lemma has been established in Moskow and Vogelius (1997) for the multi-dimensional case, we provide a notation-specific proof for completeness. Consider the weak form of the first two cell problems, (9) and (10), given by

$$\text{Find } P_j \in \mathcal{V} \ \text{ s.th. } \quad \int_0^1 \hat{E} P_{j,y}\, w_{,y} \, \mathrm{d}y = F_j(w) \quad \forall w \in \mathcal{V}, \qquad j = 1, 2 \tag{14}$$

where

$$\mathcal{V} = \big\{ w \in H^1(Y) : w \text{ is } Y\text{-periodic and } \langle w \rangle = 0 \big\},$$

and

$$F_1(w) = -\int_0^1 \hat{E} w_{,y} \, \mathrm{d}y, \qquad F_2(w) = -\int_0^1 \Big(\hat{E} P_1 w_{,y} + \mathcal{E}_0 \frac{\hat{\rho}}{\varrho_0} w - \hat{E}\,\big(1 + P_{1,y}\big)\, w \Big) \, \mathrm{d}y.$$

On setting $w = P_2$ (resp. $w = P_1$) in (14) for $j = 1$ (resp. $j = 2$) and noting the equality of thus created left-hand sides, one obtains $F_1(P_2) = F_2(P_1)$ and consequently

$$\int_0^1 \hat{E}\,\big(P_1 + P_{2,y}\big) \ \mathrm{d}y \ = \ \mathcal{E}_0 \int_0^1 \frac{\hat{\rho}}{\varrho_0} P_1 \, \mathrm{d}y. \tag{15}$$

Thanks to the definition (12) of $\mathcal{E}_1$ and ϱ_1, (15) immediately recovers (13). □

2.3. Mean fields and homogenized equations

Once the foregoing cell functions are computed, the evaluation of u_j ($j = \overline{0,2}$) in (8) requires knowledge of the mean fields U_j. Once again, inserting expansion (7) into (6) and averaging with respect to y Wautier and Guzina (2015) leads to a cascade of "macroscopic" field equations

$$\begin{aligned} O(1): &\quad \mathcal{E}_0 U_{0,xx} + \varrho_0 \omega^2 U_0 = 0, \\ O(\varepsilon): &\quad \mathcal{E}_0 U_{1,xx} + \varrho_0 \omega^2 U_1 + \mathcal{E}_1 U_{0,xxx} + \varrho_1 \omega^2 U_{0,x} = 0, \\ O(\varepsilon^2): &\quad \mathcal{E}_0 U_{2,xx} + \varrho_0 \omega^2 U_2 + \mathcal{E}_1 U_{1,xxx} + \varrho_1 \omega^2 U_{1,x} + \mathcal{E}_2 U_{0,xxxx} + \varrho_2 \omega^2 U_{0,xx} = 0. \end{aligned} \tag{16}$$

Thanks to Lemma 1, however, one has

$$\mathcal{E}_1 U_{0,xxx} + \varrho_1 \omega^2 U_{0,x} \;=\; \frac{\varrho_1}{\varrho_0}(\mathcal{E}_0 U_{0,xx} + \varrho_0 \omega^2 U_0)_{,x} \;=\; 0.$$

On letting

$$k_0 = \frac{\omega}{c_0}, \qquad c_0 = \sqrt{\frac{\mathcal{E}_0}{\varrho_0}},$$

we accordingly obtain

$$\begin{aligned} O(1): &\quad U_{0,xx} + k_0^2\, U_0 = 0, \\ O(\varepsilon): &\quad U_{1,xx} + k_0^2\, U_1 = 0, \\ O(\varepsilon^2): &\quad U_{2,xx} + k_0^2\, U_2 + \frac{\mathcal{E}_2}{\mathcal{E}_0} U_{0,xxxx} + \frac{\varrho_2}{\varrho_0} k_0^2\, U_{0,xx} = 0. \end{aligned} \tag{17}$$

By analogy to (7), we define the successive mean-field approximations $U^{(p)}$ as finite sums $\sum_{j=0}^{p} \varepsilon^j U_j$. In particular, we write

$$U^{(1)}(x) = U_0(x) + \varepsilon U_1(x), \qquad U^{(2)}(x) = U_0(x) + \varepsilon U_1(x) + \varepsilon^2 U_2(x).$$

From the weighted sum of (17) one finds that $U^{(2)}$ solves

$$U^{(2)}_{,xx} + k_0^2\, U^{(2)} + \varepsilon^2 \left[\frac{\mathcal{E}_2}{\mathcal{E}_0} U^{(2)}_{,xxxx} + \frac{\varrho_2}{\varrho_0} k_0^2\, U^{(2)}_{,xx} \right] = 0, \tag{18}$$

up to an $O(\varepsilon^3)$ residual. By utilizing the $O(1)$ equation in (16) to further approximate the $O(\varepsilon^2)$ term in (18) as in Wautier and Guzina (2015), we obtain a *family* of the mean field equations

$$U^{(2)}_{,xx} \;+\; k_0^2\, U^{(2)} \;+\; \varepsilon^2 \left(\beta_x U^{(2)}_{,xxxx} + \beta_m k_0^2\, U^{(2)}_{,xx} - \beta_t k_0^4\, U^{(2)} \right) \;=\; 0, \tag{19}$$

where β_x, β_m and β_t are subject to the constraint

$$\beta_x - \beta_m - \beta_t \;=\; \frac{\mathcal{E}_2}{\mathcal{E}_0} - \frac{\varrho_2}{\varrho_0}.$$

For future reference, (19) can be conveniently rearranged as

$$\varepsilon^2 \beta_x U^{(2)}_{,xxxx} \;+\; \left(1 + \varepsilon^2 \beta_m k_0^2\right) U^{(2)}_{,xx} \;+\; k_0^2 \left(1 - \varepsilon^2 \beta_t k_0^2\right) U^{(2)} \;=\; 0. \tag{20}$$

The elemental members of family (20) are obtained by setting any two entries of the triplet $(\beta_x, \beta_m, \beta_t)$ identically to zero. Such models with $\beta_x \neq 0$, $\beta_m \neq 0$, and $\beta_t \neq 0$ will be referred to respectively as the "space" (x), "mixed" (m), and "time" (t) models. In particular, the (m) model has been proposed and studied in previous works (e.g. Fish et al., 2002; Lamacz, 2011) and will be used as the reference elemental model hereafter.

Similarly, models obtained by discarding a single entry of the triplet $(\beta_x, \beta_m, \beta_t)$ will be denoted as (mt), (xt) and (xm). In what follows, we focus our attention on the (mt) model

$$U^{(2)}_{,xx} \;+\; k_0^2\, \frac{1 - \varepsilon^2 \beta_t k_0^2}{1 + \varepsilon^2 \beta_m k_0^2}\, U^{(2)} = 0, \qquad \beta_m + \beta_t = \frac{\varrho_2}{\varrho_0} - \frac{\mathcal{E}_2}{\mathcal{E}_0}, \tag{21}$$

that excludes the fourth-order spatial derivative. Finally, notation (xmt) will be used to designate the general model (20) featuring all three β coefficients. Some of these models and their utility in describing the dispersive behavior of periodic structures will be addressed in Section 4 for an example periodic structure.

2.4. Cell stresses and stress expansion

Inspired by the structure of (9)–(11), we consider the *cell stresses* $\Sigma_j(y)$ ($j = \overline{0,2}$) given by

$$\Sigma_j = \frac{\hat{E}}{\mathcal{E}_0}\big(P_j + P_{j+1,y}\big), \quad j = \overline{0,2}, \tag{22}$$

recalling that $P_0 = 1$. By virtue of (9)–(12), one finds that $\Sigma_0(y) = 1$ and further

$$\Sigma_{0,y} = 0, \qquad \Sigma_{1,y} = \frac{\hat{\rho}}{\varrho_0} - \Sigma_0, \qquad \Sigma_{2,y} = \frac{\hat{\rho}}{\varrho_0} P_1 - \Sigma_1, \qquad \langle \Sigma_j \rangle = \frac{\mathcal{E}_j}{\mathcal{E}_0}. \tag{23}$$

For clarity of presentation, however, we will keep the symbol Σ_0 wherever it formally appears. The key utility of (22) is that the axial stress stemming from $\hat{u}(x,y)$, see (5) and (7), can be expanded as

$$\hat{\sigma}(x,y) \;=\; \hat{E}(y)\frac{\mathrm{d}}{\mathrm{d}x}\hat{u}(x,y) \;=\; \mathcal{E}_0\left[U^{(2)}_{,x}(x)\Sigma_0(y) + \varepsilon U^{(1)}_{,xx}(x)\Sigma_1(y) + \varepsilon^2 U_{0,xxx}(x)\Sigma_2(y) + O(\varepsilon^3)\right]. \tag{24}$$

3. Homogenized boundary and transmission conditions

To introduce the effective boundary conditions completing the mean-field equations (20) and (21), we next investigate the solutions of a *model*, single-scale boundary value problem (BVP) describing a rod that is clamped at $x = 0$ and subjected to time-harmonic traction σ_L at $x = L$. An extension of the featured results to transmission conditions is discussed at the end of this section.

With reference to the original field equation (2), the model BVP reads

$$\begin{aligned} &(E(x)u_{,x})_{,x} + \rho(x)\,\omega^2 u = 0 && \text{for } x \in Y_L, \\ &u = 0 && \text{at } x = 0, \\ &\sigma = E(x)u_{,x} = \sigma_L && \text{at } x = L, \end{aligned} \tag{25}$$

where

$$Y_L = \{x \in \mathbb{R} : 0 < x < L\}.$$

For future reference, we first investigate the well-posedness of this problem. The solution u satisfies the variational equation

$$a(u,v) = F(v) \quad \forall v \in V \tag{26}$$

with

$$V = \{v \in H^1(Y_L) :\; v(0) = 0\},$$

and

$$a(u,v) = \int_0^L E\,u_{,x}v_{,x}\,\mathrm{d}x \;-\; \omega^2 \int_0^L \rho\,uv\,\mathrm{d}x, \qquad F(v) = \sigma_L v(L).$$

It is known (see for instance (McLean, 2000, Thm. 4.2) or adapt (Brezis, 2011, Thm. 8.22) to the present case) that the homogeneous counterpart of (25) (with $\sigma_L = 0$) has a countable set of positive real eigenvalues, $\lambda_j = \omega_j^2 > 0$, such that $\lambda_j \to +\infty$ as $j \to +\infty$. Assuming that $\omega \neq \omega_j$, (25) consequently admits at most one solution. Further, thanks to the bounds in (1) on the material properties and the normalization scheme adopted in Remark 1, operator $a(\cdot,\cdot)$ satisfies the Gårding inequality

$$\big|a(u,u) + 2\omega^2\|u\|_0\big| \;\geqslant\; \min(1,\omega^2)\|u\|_1 \tag{27}$$

where

$$\|\cdot\|_p \;=\; \|\cdot\|_{H^p(Y_L)},$$

and in particular $\|\cdot\|_0 = \|\cdot\|_{L^2(Y_L)}$.

By (27), the classical Fredholm theory ensures that (26) is uniquely solvable, i.e. that the inverse map $A^{-1} : \sigma_L \mapsto u$ exists. Moreover, since the forward operator $a(\cdot,\cdot)$ is bounded, so is A^{-1}. As a result, we have the stability result

$$\|u\|_1 \leqslant C\,|\sigma_L| \tag{28}$$

for some constant $C > 0$ that depends on frequency ω, but not on the cell size ε of periodic microstructure.

3.1. Leading-order homogenization

We first recall the system satisfied by the leading-order approximation $U^{(0)} = U_0 = u_0$ of the exact solution u:

$$\begin{aligned} &U^{(0)}_{,xx} + k_0^2\, U^{(0)} = 0 \quad && \text{for } x \in Y_L, \\ &U^{(0)} = 0 && \text{at } x = 0, \\ &\mathcal{E}_0 U^{(0)}_{,x} = \sigma_L && \text{at } x = L. \end{aligned} \tag{29}$$

This system is obtained by (i) using the bulk equation (17) satisfied by $U^{(0)}$ and (ii) applying the displacement and stress boundary conditions to the leading-order approximations $U^{(0)}$ and $\sigma^{(0)} = \mathcal{E}_0 U^{(0)}_{,x}$. It is well-known (e.g. Cioranescu and Donato (1999)) that u converges to $U^{(0)}$ as $\varepsilon \to 0$ in L^2-norm; more precisely, one has the estimate:

$$\exists C > 0 \quad s.th. \quad \|u - U^{(0)}\|_0 \leqslant C\varepsilon \|U^{(0)}\|_0.$$

It should be noted, however, that there is no convergence in H^1-norm (i.e. the derivatives of the fields $U^{(0)}$ and u do not match as $\varepsilon \to 0$), due to the absence of correctors accounting for the fast oscillations of the microstructure and therefore of the exact solution u. In unbounded domains, the convergence result is obtained (and the convergence rate is increased in terms of both norms) by adding the bulk correctors and correcting the wave equation as discussed in the previous section, see e.g. Lamacz (2011). In bounded domains, however, the convergence is constrained by boundary layer effects and appropriate boundary correctors must accompany the bulk corrections, as discussed now.

3.2. Background on boundary correctors and hypotheses made in the present setting

In a general multi-dimensional setting, deriving appropriate boundary conditions for higher-order homogenized models in domain $\Omega \subset \mathbb{R}^d$, $d \geqslant 2$ is a complex problem that is still an active research topic (e.g. Gérard-Varet and Masmoudi, 2012). Indeed, while accounting for higher-order terms (say $u_1(x, y)$) in the two-scale expansion, one must consider a rapidly oscillating behavior of the trace of these terms on $\partial\Omega$ and study the *boundary layer* in the vicinity of this boundary. Rigorous convergence analysis is therefore possible by introducing additional functions in the expansion: the so-called *boundary correctors* θ_j^ε, which were studied in Dumontet (1986); Santosa and Vogelius (1993); Moskow and Vogelius (1997); Allaire and Amar (1999); Gérard-Varet and Masmoudi (2012); Armstrong et al. (2017) among many others, and extended recently to transmission problems (Cakoni et al. (2016); Lin and Meng (2019); Cakoni et al. (2019)).

However, these correctors are solutions of boundary value problems posed for the *periodic* (as opposed to homogenized) medium, and a separate asymptotic procedure is required to provide the effective boundary conditions for BVPs governing the mean fields. In particular, in Santosa and Vogelius (1993) it is shown that for polygonal domains with rational slopes, *including one-dimensional problems as a particular case*, the limit θ_j^* of θ_j^ε as $\varepsilon \to 0$ may not be unique and depends on the sequence of ε_j's chosen to establish such a limit, see also the recent analyses Cakoni et al. (2016, 2019) of transmission problems.

In the case of one-dimensional problems, however, some of these difficulties can be avoided. First, the boundary data at $x = 0$ and $x = L$ are numbers. In this work, we make an additional simplifying assumption that the domain Y_L is composed of an integer number N of unit cells, i.e. that

$$\varepsilon = \frac{L}{N}, \quad N \in \mathbb{N}^+. \tag{30}$$

Accordingly, the numerical convergence results presented later on reflect (30) in that $\varepsilon \to 0$ stands for $N \to +\infty$, with ω being fixed. Consequently, the boundary values of the displacement and stress expansions, (7) and (24), are obtained by evaluating the mean fields $U^{(j)}$ and their derivatives at $x \in \{0, L\}$, the cell functions P_j and the cell stresses Σ_j at $y = 0$. The values $P_j(0)$ and $\Sigma_j(0)$ thus act as fixed coefficients that define enriched boundary conditions for the mean fields.

Remark 2. *Note that choosing "microscopically" different points as domain boundaries could be easily handled. For instance, if $x = L$ corresponds to $y = y_L$ inside the last cell, one has to replace the coefficients $P_j(0)$ and $\Sigma_j(0)$ respectively by $P_j(y_L)$ and $\Sigma_j(y_L)$ in the enhanced boundary conditions, see also Maurel and Marigo (2018) for a related study.*

For completeness, we also note that when $\beta_x \neq 0$, the field equations (20) feature the fourth-order derivative $U^{(2)}_{,xxxx}$; as a result, this class of field equations necessitates *additional boundary conditions* (BCs) compared to the original problem (25). In Askes et al. (2008), such conditions are derived from the variational formulation in terms of $U^{(2)}$ so that the boundary contributions cancel in the bilinear form associated with (20) and the resulting problem is well-posed. The coefficients featured by the germane boundary conditions are thus notably affected by the choice of the field equation. Leaning on a more physical argument, the study in Kaplunov and Pichugin (2009) focuses on the presence of *extraneous* (non-physical) solutions to (20) and the necessity to take them into account while formulating the relevant boundary conditions (typically, by introducing BCs that cancel the extraneous waves). However, no error analysis is provided with such boundary conditions, and it is not clear at this point how to make a rigorous link between them and the convergence results underlying the homogenization theory.

Remark 3. *In what follows, we focus on the second-order effective analysis of the (mt) model, i.e. we set $\beta_x = 0$ which eliminates the $U^{(2)}_{,xxxx}$ term and synthesizes the germane dispersion effects in terms of $k_0^2 U^{(2)}_{,xx}$ and $k_0^4 U^{(2)}$ instead. As shown below, such hypothesis allows us to establish the convergence results similar to those in Moskow and Vogelius (1997) for suitably chosen first- and second-order approximations of the displacement field $u(x)$ and stress field $\sigma(x)$. To clarify the nomenclature, we refer to $U^{(0)}$, $\hat{u}^{(1)}$ and $\hat{u}^{(2)}$ in (7) as the zeroth-, first-, and second-order approximations of $\hat{u}(x,y)$, respectively.*

3.3. First-order model

Motivated by the two-scale expansions (7) and (24), we introduce the first-order approximations of the (single-scale) displacement field $u(x)$ and stress field $\sigma(x)$ solving (25) respectively as

$$\begin{aligned} \tilde{u}^{(1)}(x) &= U^{(1)}(x) + \varepsilon P_1(x/\varepsilon) U^{(1)}_{,x}(x), \\ \tilde{\sigma}^{(1)}(x) &= \mathcal{E}_0\big[\Sigma_0 U^{(1)}_{,x}(x) + \varepsilon \Sigma_1(x/\varepsilon) U^{(1)}_{,xx}(x)\big], \end{aligned} \tag{31}$$

where $\Sigma_0 = 1$ as examined earlier. The mean field $U^{(1)}$, which includes an $O(\varepsilon)$ correction, is then defined as the solution of the BVP obtained by: (i) considering the zeroth-order effective field equation over Y_L (note that the $O(\varepsilon)$ correction in (21) is zero), and (ii) requiring $\tilde{u}^{(1)}$ and $\tilde{\sigma}^{(1)}$ to satisfy the exact boundary conditions in (25), namely

$$\begin{aligned} &U^{(1)}_{,xx} + k_0^2\, U^{(1)} = 0 && \text{for } x \in Y_L, \\ &U^{(1)} + \varepsilon P_1(0) U^{(1)}_{,x} = 0 && \text{at } x = 0, \\ &\Sigma_0 U^{(1)}_{,x} - \varepsilon k_0^2\, \Sigma_1(0) U^{(1)} = \sigma_L/\mathcal{E}_0 && \text{at } x = L. \end{aligned} \tag{32}$$

Note that we used the field equation $U^{(1)}_{,xx} = -k_0^2\, U^{(1)}$ in the stress boundary condition, thus obtaining Robin-like boundary conditions at both ends – which simplifies the numerical treatment. In what follows, the $O(\varepsilon)$ contributions to the boundary conditions will be referred to as *boundary correctors*. Their specific role in the asymptotic approximation will be highlighted later. Concerning the exact BVP (25), we assume from the onset that k_0 is not an eigenvalue of (32); as a result, $U^{(1)}$ is uniquely defined and depends continuously on σ_L. Further since the problem is free of body forces, we have that $U^{(1)} \in C^\infty(Y_L)$ whereby $\tilde{u}^{(1)}$, $\tilde{\sigma}^{(1)}$, and their derivatives are well-defined. A first estimate of the quality of approximation given by (31) and (32) is given by the following lemma.

Lemma 2. *The first-order approximation $\tilde{u}^{(1)} := U^{(1)} + \varepsilon P_1(\cdot/\varepsilon) U^{(1)}_{,x}$ of u, defined in terms of the first-order mean field $U^{(1)}$ solving (32) satisfies:*

$$\exists C > 0 \quad s.th. \quad \|u - \tilde{u}^{(1)}\|_1 \leqslant C\varepsilon \|U^{(1)}\|_1. \tag{33}$$

Proof. The proof of this lemma closely follows that of a similar result in (Moskow and Vogelius, 1997, Proposition 2.1). We first introduce the displacement and stress approximation errors as

$$\begin{aligned} v^\varepsilon &= u - \tilde{u}^{(1)} = u - U^{(1)} - \varepsilon P_1(\cdot/\varepsilon) U^{(1)}_{,x}, \\ s^\varepsilon &= \sigma - \tilde{\sigma}^{(1)} = \sigma - \mathcal{E}_0\big[\Sigma_0 U^{(1)}_{,x} + \varepsilon \Sigma_1(\cdot/\varepsilon) U^{(1)}_{,xx}\big]. \end{aligned}$$

Differentiating these fields and making use of (23) yields the relations

$$\begin{aligned} E v^\varepsilon_{,x} &= s^\varepsilon + \varepsilon s^{(1)}, & s^{(1)} &= -k_0^2\, E P_{2,y}(\cdot/\varepsilon) U^{(1)}, \\ s^\varepsilon_{,x} &= -\omega^2(\rho v^\varepsilon + \varepsilon \varrho_0 v^{(1)}), & v^{(1)} &= \Sigma_{2,y}(\cdot/\varepsilon) U^{(1)}_{,x}, \end{aligned} \tag{34}$$

noting from the boundary conditions in (25) and (32) that

$$v^\varepsilon(0) = 0 \qquad \text{and} \qquad s^\varepsilon(L) = 0. \tag{35}$$

To establish estimate (33), we next aim to evaluate the duality product (v^ε, ϕ) (identified with the L^2 inner product) for $\phi \in H^{-1}(Y_L)$. To this end, we introduce function w as the solution of a BVP for the periodic medium with source term ϕ in the weak sense. Slightly abusing the notation, we write

$$\begin{aligned} &(E(x)w_{,x})_{,x} + \rho(x)\omega^2 w = \phi \quad && \text{for } x \in Y_L, \\ &w = 0 && \text{at } x = 0, \\ &E(x)w_{,x} = 0 && \text{at } x = L. \end{aligned} \tag{36}$$

This problem is nearly identical to the model problem (25), except for the non-trivial source term ϕ and homogeneous boundary condition at $x = L$. Using the same arguments as in the stability analysis of (25) resulting in (28), we obtain

$$\exists C > 0 \quad s.th. \quad \|w\|_1 < C\|\phi\|_{-1}. \tag{37}$$

With the aid of (34), we then compute

$$\begin{aligned} (v^\varepsilon, \phi) &= \int_0^L v^\varepsilon \big((Ew_{,x})_{,x} + \rho\omega^2 w\big)\, \mathrm{d}x \\ &= [Ew_{,x}v^\varepsilon]_0^L - \int_0^L \big((s^\varepsilon + \varepsilon s^{(1)})w_{,x} - \rho\omega^2 v^\varepsilon w\big)\, \mathrm{d}x \\ &= [Ew_{,x}v^\varepsilon]_0^L - [s^\varepsilon w]_0^L - \varepsilon \int_0^L (s^{(1)}w_{,x} + \varrho_0\omega^2 v^{(1)} w)\, \mathrm{d}x. \end{aligned} \tag{38}$$

Thanks to the homogeneous boundary conditions (35) and those in (36), the boundary terms in (38) vanish; using the expressions in (34) for $s^{(1)}$ and $v^{(1)}$, we consequently obtain

$$(v^\varepsilon, \phi) = \varepsilon k_0^2 \int_0^L \big(EP_{2,y}(\cdot/\varepsilon)U^{(1)}w_{,x} - \mathcal{E}_0\Sigma_{2,y}(\cdot/\varepsilon)U^{(1)}_{,x}w\big)\, \mathrm{d}x.$$

Since the functions $E(x)$, $x \mapsto P_{2,y}(x/\varepsilon)$, and $x \mapsto \Sigma_{2,y}(x/\varepsilon)$ are bounded (independent of ε), we find that

$$\exists C_1, C_2 > 0 \quad s.th. \quad |(v^\varepsilon, \phi)| \leqslant C_1\varepsilon\|U^{(1)}\|_1\|w\|_1 \leqslant C_2\varepsilon\|U^{(1)}\|_1\|\phi\|_{-1}, \tag{39}$$

where we used (37) for the second inequality. Then, since (39) holds for any $\phi \in H^{-1}(Y_L)$, we use the result

$$\|z^\varepsilon\|_1 = \max_{\substack{\phi \in H^{-1}(Y_L) \\ \|\phi\|_{-1}=1}} |(v^\varepsilon, \phi)|$$

established in (Brezis, 2011, Corollary 1.4) to conclude the proof. □

Remark 4. *Result (33) is classical for 1D homogenization problems, and in fact it does not require the use of boundary correctors. Indeed, without such correctors, the contribution of the boundary terms in (38) does not vanish but becomes $O(\varepsilon)$. In higher dimensions, however, oscillating behavior of the like boundary terms results in an $O(\varepsilon^{1/2})$ error in terms of the germane $H^1(\Omega)$-norm – unless the boundary correctors are deployed, see (Cioranescu and Donato, 1999, Theorem 6.3). Notwithstanding such 1D result, the role of the boundary correctors in (32) becomes clear when considering the L^2-error, $\|u - \tilde{u}^{(1)}\|_0$, featured by the second-order approximation that is pursued next.*

3.4. Second-order model

We next proceed with the second-order homogenization by following the steps outlined in Section 3.3. Specifically, we seek the second-order approximations of $u(x)$ and $\sigma(x)$ as

$$\begin{aligned} \tilde{u}^{(2)}(x) &= U^{(2)}(x) + \varepsilon P_1(x/\varepsilon)U^{(2)}_{,x}(x) + \varepsilon^2 P_2(x/\varepsilon)U^{(2)}_{,xx}(x), \\ \tilde{\sigma}^{(2)}(x) &= \mathcal{E}_0\big[\Sigma_0 U^{(2)}_{,x} + \varepsilon\Sigma_1(x/\varepsilon)U^{(2)}_{,xx}(x) + \varepsilon^2\Sigma_2(x/\varepsilon)U^{(2)}_{,xxx}(x)\big], \end{aligned} \tag{40}$$

where the second-order mean field $U^{(2)}$, defined using the "mixed" (mt) model for the bulk equation, solves the BVP

$$\begin{aligned} &U^{(2)}_{,xx} + k_{mt}^2 U^{(2)} = 0 && \text{for } x \in Y_L, \\ &\big[1 - \varepsilon^2 k_{mt}^2 P_2(0)\big] U^{(2)} + \varepsilon P_1(0) U^{(2)}_{,x} = 0 && \text{at } x = 0, \\ &\big[\Sigma_0 - \varepsilon^2 k_{mt}^2 \Sigma_2(0)\big] U^{(2)}_{,x} - \varepsilon k_{mt}^2 \Sigma_1(0) U^{(2)} = \sigma_L/\mathcal{E}_0 && \text{at } x = L, \end{aligned} \tag{41}$$

with

$$k_{mt}^2 = k_{mt}^2(\varepsilon) \;=\; k_0^2 \, \frac{1 - \varepsilon^2 \beta_t k_0^2}{1 + \varepsilon^2 \beta_m k_0^2}. \tag{42}$$

We first note that (41) features *Robin-like* boundary condtions, similar to its first-order companion (32). As expected, by (40)–(42) we improve the approximation in the following sense.

Lemma 3. *The second-order approximation* $\tilde{u}^{(2)} = U^{(2)} + \varepsilon P_1(\cdot/\varepsilon) U^{(2)}_{,x} + \varepsilon^2 P_2(\cdot/\varepsilon) U^{(2)}_{,xx}$ *of* u*, given in terms of the second-order mean field* $U^{(2)}$ *solving* (41)*, is such that*

$$\exists C > 0 \quad s.th. \quad \|u - \tilde{u}^{(2)}\|_1 \leqslant C\varepsilon^2 \|U^{(2)}\|_1. \tag{43}$$

Proof. As before, we define the respective displacement and stress approximation errors as

$$\begin{aligned} v^\varepsilon &= u - \tilde{u}^{(2)}, \\ s^\varepsilon &= \sigma - \tilde{\sigma}^{(2)}, \end{aligned}$$

noting from the boundary conditions in (25) and (41) that

$$v^\varepsilon(0) = 0 \qquad \text{and} \qquad s^\varepsilon(L) = 0.$$

On differentiating these errors and making use of (23), we obtain

$$\begin{aligned} E v^\varepsilon_{,x} &= s^\varepsilon + \varepsilon^2 s^{(2)}, & s^{(2)} &= -k_{mt}^2 E P_{3,y}(\cdot/\varepsilon) U^{(2)}_{,x}, \\ s^\varepsilon_{,x} &= -\omega^2 \big(\rho v^\varepsilon + \varepsilon^2 \varrho_0 v^{(2)} + \rho v_{mt}\big), & v^{(2)} &= k_{mt}^2 \big[k_0^{-2} k_{mt}^2 \Sigma_2(\cdot/\varepsilon) - \varrho_0^{-1} \rho P_2(\cdot/\varepsilon)\big] U^{(2)}, \\ & & v_{mt} &= (1 - k_0^{-2} k_{mt}^2) \big[U^{(2)} + \varepsilon P_1(\cdot/\varepsilon) U^{(2)}_{,x}\big]. \end{aligned}$$

In the above decomposition of $s^\varepsilon_{,x}$, it is clear that $v^{(2)} = O(1)$ and $v_{mt} = O(1 - k_{mt}^2/k_0^2) = O(\varepsilon^2)$ as $\varepsilon \to 0$ by the Taylor expansion of (42). The remainder of the proof follows that of Lemma 2, except that the remainders due to errors v^ε and s^ε are $O(\varepsilon^2)$, yielding the estimate (43). □

Recalling Remark 4, we are now in position to establish the main result of this section.

Theorem 4. *The first-order approximation* $\tilde{u}^{(1)} = U^{(1)} + \varepsilon P_1(\cdot/\varepsilon) U^{(1)}_{,x}$ *of* u*, where* $U^{(1)}$ *solves the homogenized problem* (32)*, satisfies both the* H^1*-norm estimate from Lemma 2 and the* L^2*-norm estimate*

$$\exists C > 0 \quad s.th. \quad \|u - \tilde{u}^{(1)}\|_0 \leqslant C\varepsilon^2 \|U^{(2)}\|_2, \tag{44}$$

where $U^{(2)}$ *solves the second-order homogenized problem* (41)*.*

Proof. The idea is to show that $\|\tilde{u}^{(1)} - \tilde{u}^{(2)}\|_0 \leqslant C\varepsilon^2 \|U^{(2)}\|_2$, which then yields (44) by Lemma 3 and triangle inequality. To this end, we let

$$\tilde{v}(x) \;=\; \tilde{u}^{(2)}(x) - \tilde{u}^{(1)}(x) \;=\; \tilde{V}(x) + \varepsilon P_1(x/\varepsilon) \tilde{V}_{,x}(x) + \varepsilon^2 P_2(x/\varepsilon) U^{(2)}(x) \tag{45}$$

where $\tilde{V} = U^{(2)} - U^{(1)}$ satisfies the difference between problems (41) and (32), namely

$$\begin{aligned} &\tilde{V}_{,xx} + k_0^2 \tilde{V} = k_0^2 \big(1 - k_{mt}^2/k_0^2\big) U^{(2)} && \text{for } x \in Y_L, \\ &\tilde{V} + \varepsilon P_1(0) \tilde{V}_{,x} = \varepsilon^2 k_{mt}^2 P_2(0) U^{(2)} && \text{at } x = 0, \\ &\Sigma_0 \tilde{V}_{,x} - \varepsilon k_0^2 \, \Sigma_1(0) \tilde{V} = \varepsilon^2 k_{mt}^2 \Sigma_2(0) U^{(2)}_{,x} - \varepsilon k_0^2 \big(1 - k_{mt}^2/k_0^2\big) \Sigma_1(0) U^{(2)} && \text{at } x = L, \end{aligned}$$

which features $U^{(2)}$ as the "source" term. Equipped with (i) the premise that k_0 is not an eigenvalue of this problem; (ii) estimate $1 - k_{mt}^2/k_0^2 = O(\varepsilon^2)$, and (iii) the fact that the boundary data feature

the derivative term $U^{(2)}_{,x}$ (hence the H^2-norm bound in inequality (44) and below), a stability analysis similar to that of (25) yields

$$\exists C > 0 \quad s.th. \quad \|\tilde{V}\|_1 \leqslant C\varepsilon^2 \|U^{(2)}\|_2.$$

Then from definition (45),

$$\exists C > 0 \quad s.th. \quad \|\tilde{v}\|_0 \leqslant C\varepsilon^2 \|U^{(2)}\|_2,$$

and finally, by Lemma 3

$$\exists C > 0 \quad s.th. \quad \|u - \tilde{u}^{(1)}\|_0 \leqslant \|u - \tilde{u}^{(2)}\|_0 + \|\tilde{v}\|_0 \leqslant C\varepsilon^2 \|U^{(2)}\|_2.$$

□

Remark 5. *Following the observation made in Remark 4, one can show that the second-order boundary correctors in (41) governing $U^{(2)}$ are not necessary to establish Lemma 3 and Theorem 4. However, these very correctors are necessary to establish the next-order estimate*

$$\exists C > 0 \quad s.th. \quad \|u - \tilde{u}^{(2)}\|_0 \leqslant C\varepsilon^3 \|U^{(3)}\|_2.$$

While we do not prove this result, we expect the same arguments to apply; indeed, as shown in the next section, we numerically observe the $O(\varepsilon^3)$ behavior of the misfit $\|u - \tilde{u}^{(2)}\|_0$.

3.5. Extension to transmission conditions

We next briefly discuss an extension of the above ideas to transmission conditions. As in the case of Dirichlet or Neumann boundary conditions, the transmission conditions can be imposed on the *total* homogenized displacements and stresses. For instance, assuming a perfect contact at $x = 0$ between the homogeneous medium ($x < 0$) and a periodic medium ($x > 0$), we have

$$u(0^-) = \tilde{u}^{(j)}(0^+) \quad \text{and} \quad \sigma(0^-) = \tilde{\sigma}^{(j)}(0^+),$$

where u and σ signify the displacement and stress in the homogeneous "background", while $\tilde{u}^{(j)}$ and $\tilde{\sigma}^{(j)}$ are their j-th order homogenized counterparts in the periodic medium. On replacing $\tilde{u}^{(j)}$ and $\tilde{\sigma}^{(j)}$ by their expansions, involving the mean field $U^{(j)}$ and germane cell solutions, we obtain two "effective" transmission conditions on the mean field, that complete the BVP featuring the homogenized wave equation in $x > 0$. An example of such exercise is provided in Appendix B.2.

For brevity, we do not provide the proofs of convergence for the transmission problem. We however expect the same arguments to hold, and indeed via numerical simulations (described next) we observe the convergence rates that are identical to those derived for the model BVP.

4. Application to periodic bilaminate

In this section, we apply the homogenization procedure to a *two-phase periodic medium* whose unit cell Y is characterized by the geometric parameter α, material parameters (E_1 and ρ_1) of the first phase, and two material contrasts, γ_E and γ_ρ. Specifically, we take the periodic Young's modulus $\hat{E}$ and mass density $\hat{\rho}$ to be piecewise-constant according to

$$\hat{E}(y) = \begin{cases} E_1, & y \in (0, \alpha) \\ \gamma_E E_1, & y \in (\alpha, 1) \end{cases}, \qquad \hat{\rho}(y) = \begin{cases} \rho_1, & y \in (0, \alpha) \\ \gamma_\rho \rho_1, & y \in (\alpha, 1) \end{cases}. \tag{46}$$

For this class of materials, the effective Young's moduli and mass densities (12) can be obtained (e.g. Wautier and Guzina, 2015) as given below. On letting

$$n_E = \frac{\gamma_E}{(1-\alpha) + \alpha\gamma_E}, \qquad n_\rho = \alpha + (1-\alpha)\gamma_\rho, \tag{47}$$

one has

$$\begin{aligned} \mathcal{E}_0 &= n_E E_1 & \mathcal{E}_1 &= 0, & \mathcal{E}_2 &= \mathcal{E}_0 \frac{n_E^2}{n_\rho} \frac{\alpha^2(1-\alpha)^2(1-\gamma_E)(1-\gamma_E\gamma_\rho)}{12\gamma_E^2}, \\ \varrho_0 &= n_\rho \rho_1 & \varrho_1 &= 0, & \varrho_2 &= -\varrho_0 \frac{n_E}{n_\rho^2} \frac{\alpha^2(1-\alpha)^2(1-\gamma_\rho)(1-\gamma_E\gamma_\rho)}{12\gamma_E}. \end{aligned} \tag{48}$$

With such definitions, the germane family of effective field equations governing $U^{(2)}$ can be written as

$$\beta_x \varepsilon^2 U^{(2)}_{,xxxx} + \left(1 + \beta_m k_0^2 \varepsilon^2\right) U^{(2)}_{,xx} + k_0^2 \left(1 - \beta_t k_0^2 \varepsilon^2\right) U^{(2)} = 0, \qquad \beta_x - \beta_m - \beta_t = \beta, \tag{49}$$

where

$$k_0^2 = \frac{\omega^2}{c_0^2} = n_0 \frac{\omega^2}{c_1^2}, \qquad \beta = \frac{\mathcal{E}_2}{\mathcal{E}_0} - \frac{\varrho_2}{\varrho_0} = \frac{1}{12}\left[\frac{\alpha(1-\alpha)(1-\gamma_E\gamma_\rho)}{n_0\gamma_E}\right]^2, \tag{50}$$

and

$$c_1 = \sqrt{\frac{E_1}{\rho_1}}, \qquad n_0 = \frac{c_1^2}{c_0^2} = \frac{E_1\varrho_0}{\rho_1\mathcal{E}_0} = \frac{n_\rho}{n_E}.$$

For completeness, the relevant cell functions and cell stresses for the bilaminate structure are provided in Appendix A.

In the sequel, we first focus on the dispersive behavior of (49), and we consider optimal (mt) and (xmt) models whose coefficients β_x, β_m and β_t (subject to the constraint $\beta_x - \beta_m - \beta_t = \beta$) are chosen to "best" approximate the exact dispersion relationship within the first Brillouin zone. Then, we deploy an optimal (mt) model and the effective boundary conditions established in Section 3 to simulate time-harmonic waves in a bounded periodic bilaminate. As the last example, we extend the foregoing homogenization strategy to approximate the *transmission conditions* featured by a finite domain containing a periodic inclusion.

4.1. Homogenized dispersive behavior

Let κ denote the effective wavenumber of elastic disturbances propagating at frequency ω through the microstructured medium (48). Then the exact dispersion relationship Wautier and Guzina (2015), obtained by the Bloch-Floquet theory, can be written as

$$\cos(\kappa\varepsilon) = (1+\chi)\cos\left[\frac{\omega\varepsilon}{c_1}\left(\alpha + \frac{1-\alpha}{\sqrt{\gamma_E/\gamma_\rho}}\right)\right] - \chi\cos\left[\frac{\omega\varepsilon}{c_1}\left(\alpha - \frac{1-\alpha}{\sqrt{\gamma_E/\gamma_\rho}}\right)\right], \tag{51}$$

where

$$\chi = \frac{1}{4}\left(\sqrt{\gamma_E\gamma_\rho} + \frac{1}{\sqrt{\gamma_E\gamma_\rho}} - 2\right).$$

On letting $U^{(2)}(x) = e^{i\kappa x}$, it is easy to show Wautier and Guzina (2015) that the second-order (xmt) homogenized models (49) yield

$$\frac{\omega\varepsilon}{c_0} = \sqrt{\frac{1 - \beta_m(\kappa\varepsilon)^2 - \sqrt{1 - 2(\beta_m + 2\beta_t)(\kappa\varepsilon)^2 + (\beta_m^2 + 4\beta_x\beta_t)(\kappa\varepsilon)^4}}{2\beta_t}}, \tag{52}$$

which provides an asymptotic description of (51) as $\kappa\varepsilon \to 0$ up to an $O((\kappa\varepsilon)^5)$ residual Wautier and Guzina (2015). In this vein, one can take advantage of the flexibility offered by the (xmt) class of models – in terms of the choice of parameters β_x, β_t and β_m – to achieve "best" overall agreement within the first Brillouin zone.

4.1.1. Optimal two-parameter model (mt)

When $\beta_x = 0$, (52) reduces to

$$\frac{\omega\varepsilon}{c_0} = \sqrt{\frac{1 - \beta_m(\kappa\varepsilon)^2 - \sqrt{1 - 2(\beta_m + 2\beta_t)(\kappa\varepsilon)^2 + \beta_m^2(\kappa\varepsilon)^4}}{2\beta_t}}. \tag{53}$$

Under the constraint $\beta_m + \beta_t + \beta = 0$, the (mt) model offers one degree of freedom when selecting β_m and β_t. To identify the optimal pair, we select to improve upon the agreement between (51) and (52) for small $\kappa\varepsilon$; an idea that originated in the context of 1D spring-mass lattices Pichugin et al. (2008). With such goal in mind, we first compute the Taylor expansion of the exact dispersion relationship (51) up to the fifth order as

$$\frac{\omega\varepsilon}{c_0} = \kappa\varepsilon - \frac{\beta}{2}(\kappa\varepsilon)^3 - \frac{\beta\left(2 - 27\beta - 8\overline{\beta}\right)}{40}(\kappa\varepsilon)^5 + O((\kappa\varepsilon)^7), \tag{54}$$

where

$$\overline{\beta} \;=\; \frac{1}{12}\Big[\frac{\alpha^2\gamma_E-(1-\alpha)^2\gamma_\rho}{n_0\gamma_E}\Big]^2 \tag{55}$$

which vanishes for $\alpha = 1/2$ and $\gamma_E = \gamma_\rho$ Dontsov et al. (2013); Cornaggia (2016). Similarly, the homogenized (mt) relationship (53) is expanded as:

$$\frac{\omega\varepsilon}{c_0} \;=\; \kappa\varepsilon \;+\; \frac{\beta_m+\beta_t}{2}(\kappa\varepsilon)^3 \;+\; \frac{(\beta_m+\beta_t)(3\beta_m+7\beta_t)}{8}(\kappa\varepsilon)^5 \;+\; O((\kappa\varepsilon)^7). \tag{56}$$

Equating the coefficients in (54) and (56) yields the existing constraint $\beta_m+\beta_t=-\beta$, together with the additional equation

$$15\beta_m+35\beta_t = 2-27\beta-8\overline{\beta}.$$

The latter two equations are solved by the optimal pair

$$\beta_m = \frac{-1-4\beta+4\overline{\beta}}{10}, \qquad \beta_t = \frac{1-6\beta-4\overline{\beta}}{10}. \tag{57}$$

4.1.2. Optimal three-parameter model (xmt)

Rather than focusing on the low-frequency accuracy ($\kappa\varepsilon\to 0$), it may be appealing to instead pursue an approximation that provides better *global fit* within the first Brillouin zone – by incorporating the onset of the first *band gap* into the optimality criterion Dontsov et al. (2013); Wautier and Guzina (2015). An obvious idea would be to match the onset of the first band gap, $\omega_{\rm BG}$, via the requirement $\omega(\kappa\varepsilon=\pi)=\omega_{\rm BG}$ Dontsov et al. (2013). Overall, this option was found in Wautier and Guzina (2015) to under-perform at low frequencies. Another possibility, explored in Wautier and Guzina (2015), is to impose the physical requirement of zero group velocity at the end of the Brillouin zone, namely

$$\left.\frac{\partial\omega}{\partial(\kappa\varepsilon)}\right|_{\kappa\varepsilon=\pi} = 0. \tag{58}$$

This choice leads to a good compromise between the low-frequency accuracy and band-gap prediction; however (58) cannot be realized by the (mt) model (53), for which the group velocity vanishes only at $\kappa\varepsilon\to\infty$. Instead, the latter optimality criterion can be satisfied by the (xmt) model Wautier and Guzina (2015), which provides a motivation for extensions of the present work to problems with a non-trivial singular perturbation $\beta_x U_{,xxxx}$ in the effective field equation (49).

4.1.3. Application to an example bilaminate

From now on, we focus on a specific bilaminate, assuming

$$(E_1,\rho_1)=\left(1,\frac{2}{3}\right), \qquad \gamma_E=6, \qquad \gamma_\rho=\frac{3}{2}, \qquad \alpha=\frac{1}{4}. \tag{59}$$

These parameters are selected to obtain the wave speed contrast $\sqrt{\gamma_E/\gamma_\rho}=2$ and impedance contrast $\sqrt{\gamma_E\gamma_\rho}=3$ between lamina, for which the maximum dispersion is reached at $\alpha\approx 0.25$ Santosa and Symes (1991). For clarity, the values of the corresponding coefficients in the homogenized models are gathered in Table 1, along with references to their analytical expressions.

To illustrate the dispersive properties of the homogenized model, Fig. 1 compares the performance of the (non-dispersive) leading-order model, the reference (m) model, the optimal (mt) model from Section 4.1.1, and its (xmt) companion from Section 4.1.2. From the display, we note that the optimal (xmt) model is the only one capable of accurately representing the dispersion curve up the band gap (as expected); however the optimal (mt) model (57), which targets the low-frequency behavior, nonetheless provides a reasonable approximation over a majority of the first Brillouin zone.

4.2. Homogenized boundary value problem

Consider the model BVP (25) for a bilaminate rod consisting of 10 unit cells, whose parameters are listed in Table 2. In this example, we have $\omega\varepsilon=3$ as indicated by the top grey square in Fig. 1. The exact solution u of this problem is obtained via the transfer matrix approach in terms of trigonometric functions within each lamina (e.g. Cornaggia, 2016, Ch. 4), see also Appendix B concerning the related

Parameters	Expressions for bilaminates	Specific values
n_E, n_ρ	(47)	$\frac{8}{3}$, $\frac{11}{8}$
$\mathcal{E}_0$, ϱ_0	(48)	$\frac{8}{3}$, $\frac{11}{12}$
β, $\overline{\beta}$	(50), (55)	$\frac{64}{3267}$, $\frac{25}{13068}$
Optimal β_m, β_t	(57)	$-\frac{53}{495}$, $\frac{1429}{16335}$
$P_1(0)$, $P_2(0)$	(A.1), (A.3)	$-\frac{5}{24}$, $\frac{113}{6336}$
$\Sigma_1(0)$, $\Sigma_2(0)$	(A.5), (A.7)	$\frac{3}{88}$, $-\frac{109}{19008}$

Table 1: Parameters of the homogenized models: expressions and values for the example bilaminate characterized by $(E_1, \rho_1) = (1, 2/3)$, $\gamma_E = 6$, $\gamma_\rho = 3/2$ and $\alpha = 1/4$.

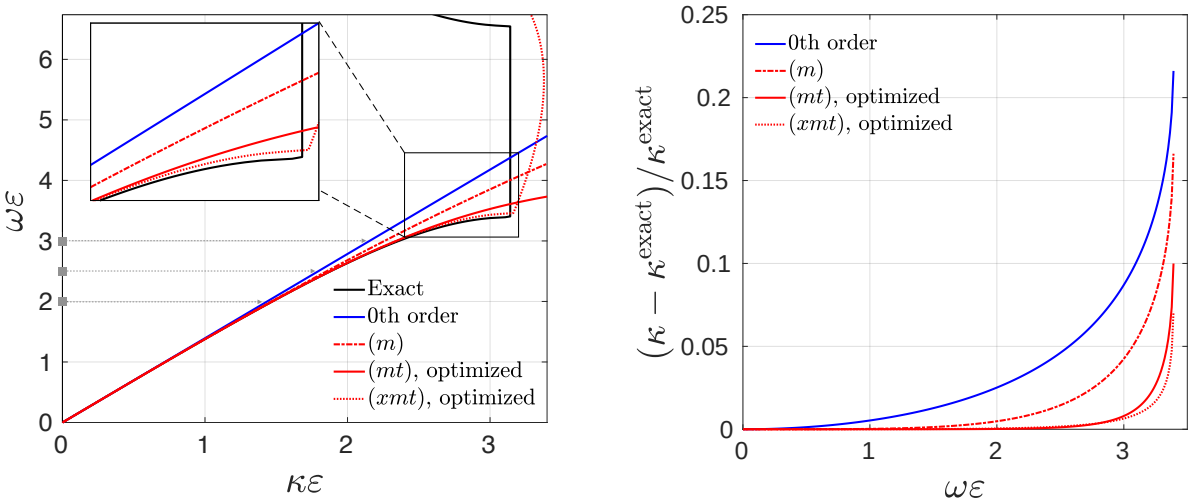

Figure 1: Dispersion relationship, up to the first band gap, for the periodic bilaminate (59): exact solution versus homogenized models. Left: $\omega\varepsilon$ versus $\kappa\varepsilon$. The grey squares indicate frequencies $\omega\varepsilon \in \{2, 2.5, 3\}$ used in the ensuing simulations. Right: Relative error on the wavenumber, $(\kappa - \kappa^{\text{exact}})/\kappa^{\text{exact}}$, versus $\omega\varepsilon$ within the first Brillouin zone.

transmission problem. To illustrate the performance of the homogenized solution, Fig. 2 first compares the mean fields $U^{(0)}$, $U^{(1)}$ and $U^{(2)}$, solving respectively (29), (32) and (41), with the exact solution u. As can be seen from the display, there is a marked improvement in the veracity of the "mean" description with increasing order of approximation. With such mean fields at hand, the "full" asymptotic approximations according to (31) and (40), namely

$$\begin{aligned} \tilde{u}^{(1)}(x) &= U^{(1)}(x) + \varepsilon P_1(x/\varepsilon) U^{(1)}_{,x}(x), \\ \tilde{u}^{(2)}(x) &= \big[1 - \varepsilon^2 k_{mt}^2 P_2(x/\varepsilon)\big] U^{(2)}(x) + \varepsilon P_1(x/\varepsilon) U^{(2)}_{,x}(x), \end{aligned} \tag{60}$$

are plotted in Fig. 3 using the cell functions P_1 and P_2 given in Appendix A. As a point of reference, included in the diagram is also the zeroth-order approximation, $\tilde{u}^{(0)}(x) = U^{(0)}(x)$. From the graph, we observe a very good qualitative agreement between $\tilde{u}^{(2)}$ and the exact solution u, while the lower-order approximations are seemingly unable to capture the fine features of the solution. A similar conclusion can be drawn from Fig. 4 which compares the exact axial stress in the rod, σ, with the asymptotic approximations $\tilde{\sigma}^{(0)} = \mathcal{E}_0 U_{0,x}$, $\tilde{\sigma}^{(1)}$ and $\tilde{\sigma}^{(2)}$, computed according to (31) and (40) using the same mean fields and the cell stresses Σ_1 and Σ_2 given in Appendix A. A common observation from Figs. 2–4 is that the error due to approximation of the *field equation* (resp. *boundary conditions*) affects primarily the *wavelenghth* (resp. *amplitude* and *phase*) of the asymptotic wavefield.

For further insight into the performance of the homogenized solution, Fig. 5 plots the relative errors

$$\frac{\|u - \tilde{u}^{(j)}\|_n}{\|u\|_n}, \qquad j = 0, 1, 2, \quad n = 0, 1$$

as $\varepsilon \to 0$ on a log-log scale (we keep the frequency fixed at $\omega = 2\pi$ while letting $N \to +\infty$ so that $\varepsilon \to 0$).

ω	L	ε	α	γ_E	γ_ρ	(E_1, ρ_1)	σ_L
2π	$30/(2\pi)$	$3/(2\pi)$	$1/4$	6	$3/2$	$(1, 2/3)$	2π

Table 2: Parameters of the model BVP (25) used in numerical simulations: $\omega\varepsilon = 3$.

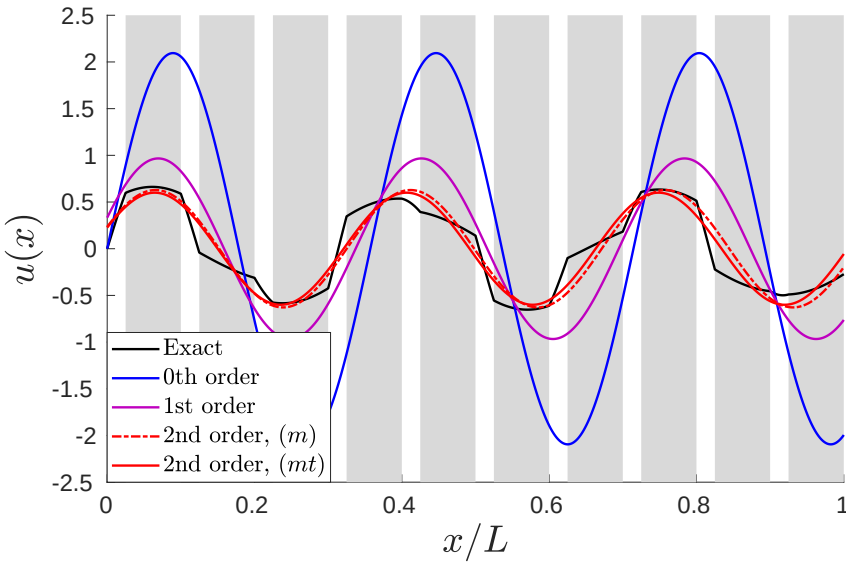

Figure 2: Exact wave motion u versus homogenized mean fields $U^{(0)}$, $U^{(1)}$ and $U^{(2)}$ for the model BVP (25) given in Table 2: excitation frequency $\omega\varepsilon = 3$. The shaded regions indicate lamina within the rod where $E = \gamma_E E_1$ and $\rho = \gamma_\rho \rho_1$.

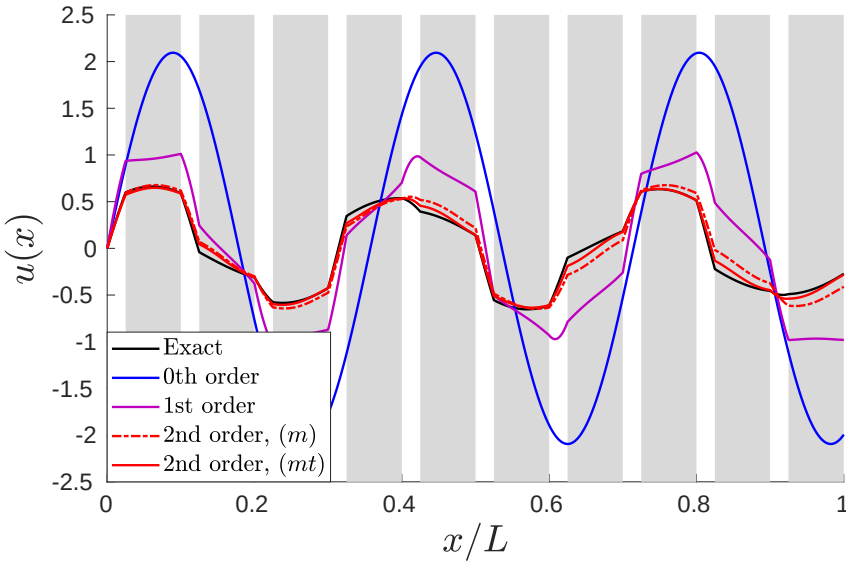

Figure 3: Exact wave motion u versus homogenized approximations $\tilde{u}^{(0)}$, $\tilde{u}^{(1)}$ and $\tilde{u}^{(2)}$ for the model BVP (25) given in Table 2: excitation frequency $\omega\varepsilon = 3$.

From the display, one clearly verifies (i) the L^2 and H^1-norm behaviors of the misfit normalized by the zeroth-order approximation $U^{(0)}$ discussed in Section 3.1; (ii) the first- and second-order H^1 estimates on $\tilde{u}^{(1)}$ and $\tilde{u}^{(2)}$ given by Lemma 2 and Lemma 3; (iii) the L^2 estimate on $\tilde{u}^{(1)}$ established in Theorem 4; and (iv) the L^2 estimate on $\tilde{u}^{(2)}$ predicted in Remark 5. As expected, the improvement brought about by the optimized (mt) model over the reference (m) model is visible only at larger values of ε. For completeness, Fig. 6 provides an analogous graph of the relative L^2 error in terms of the homogenized stress approximation, $\tilde{\sigma}^{(j)}$.

To highlight the role of boundary effects in the asymptotic approximation, we next consider a lower excitation frequency, $\omega\varepsilon = 2$, according to Table 3. In this case – indicated by the bottom grey square in Fig. 1, the dispersion effects are *negligible* and the approximation error is *dominated by the boundary effects*. Fig. 7 and Fig. 8 compare respectively the exact solution at $\omega\varepsilon = 2$ versus (i) homogenized mean

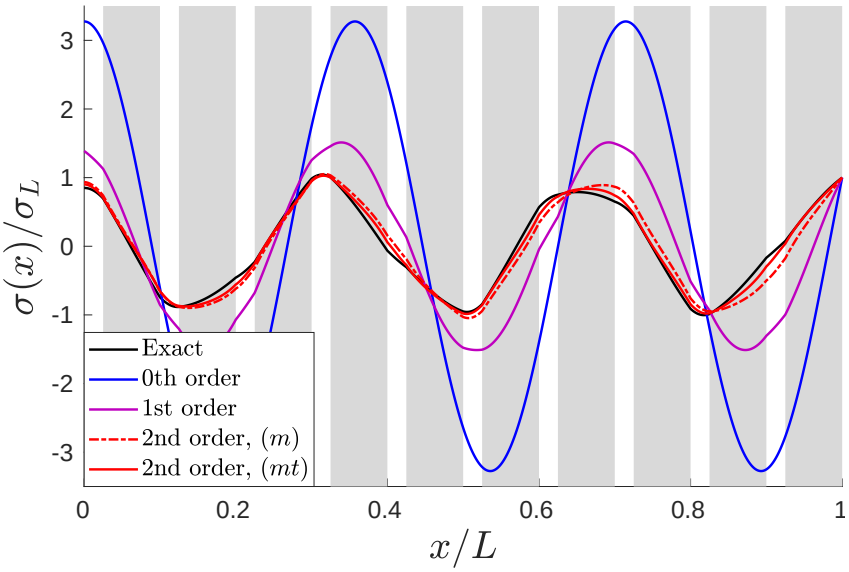

Figure 4: Exact normalized stress field σ versus homogenized approximations $\tilde{\sigma}^{(0)}$, $\tilde{\sigma}^{(1)}$ and $\tilde{\sigma}^{(2)}$ for the model BVP (25) given in Table 2: excitation frequency $\omega\varepsilon = 3$.

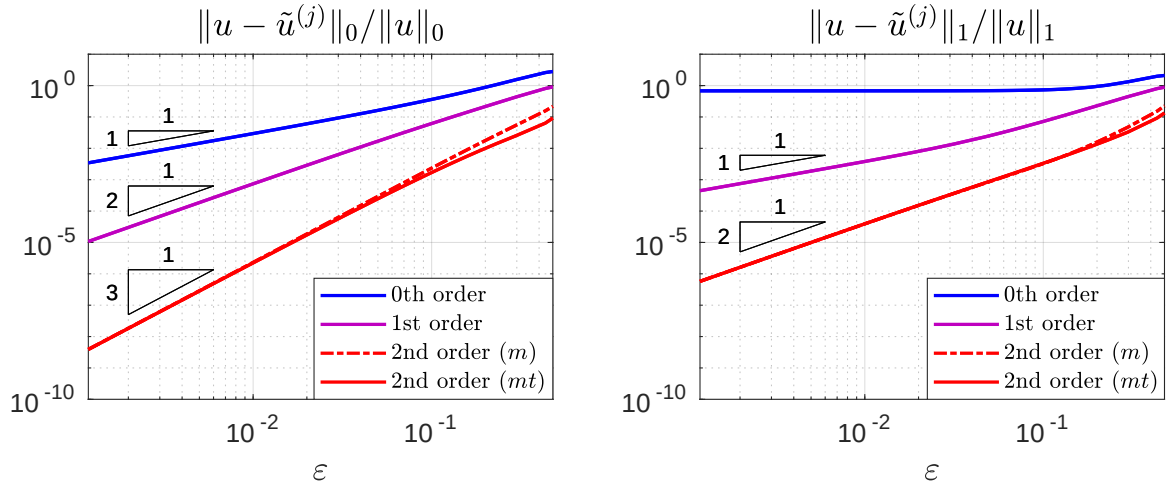

Figure 5: Relative L^2 and H^1 errors of the homogenized approximations $\tilde{u}^{(j)}$ $(j = 0, 1, 2)$ versus ε for the model BVP (25) given in Table 2.

fields $U^{(0)}$, $U^{(1)}$ and $U^{(2)}$, and (ii) homogenized approximations $\tilde{u}^{(0)}$, $\tilde{u}^{(1)}$ and $\tilde{u}^{(2)}$. As can be seen from the display, the errors generated by the zeroth- and first-order approximations are significant, while $U^{(2)}$ and especially $\tilde{u}^{(2)}$ provide a close approximation of the exact wavefield.

ω	L	ε	α	γ_E	γ_ρ	(E_1, ρ_1)	σ_L
2π	$10/\pi$	$1/\pi$	$1/4$	6	$3/2$	$(1, 2/3)$	2π

Table 3: Parameters of the model BVP (25) used in numerical simulations: $\omega\varepsilon = 2$.

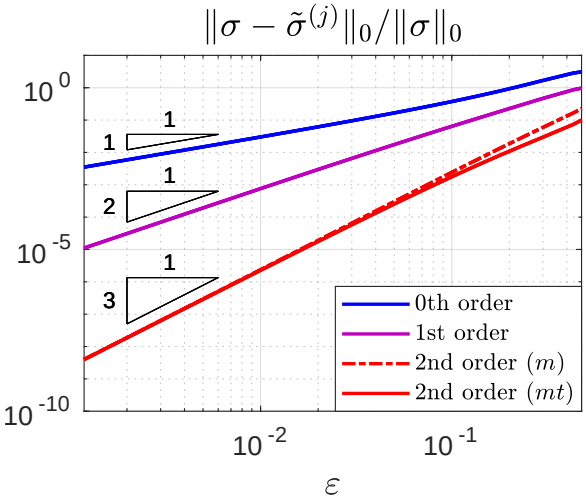

Figure 6: Relative L^2 error of the homogenized stress approximation $\tilde{\sigma}^{(j)}$ $(j = 0, 1, 2)$ versus ε for the model BVP (25) given in Table 2.

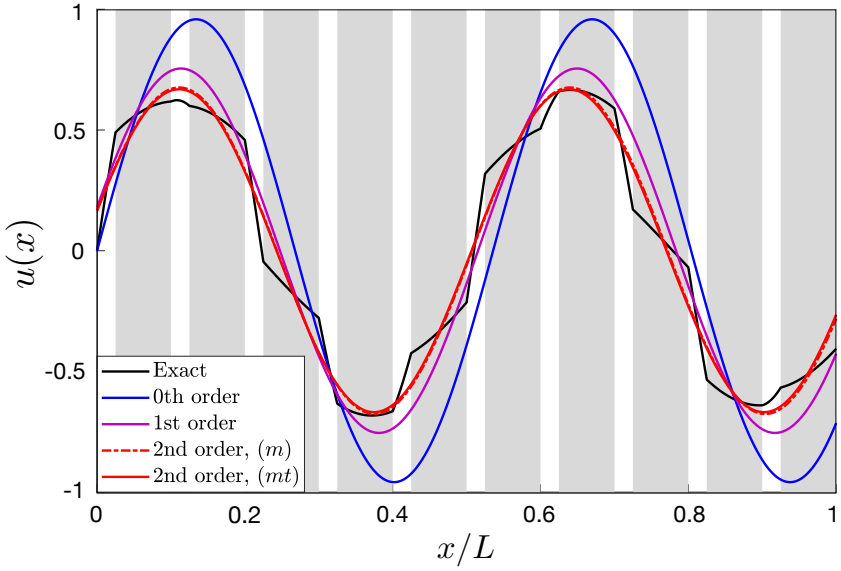

Figure 7: Exact wave motion u versus homogenized mean fields $U^{(0)}$, $U^{(1)}$ and $U^{(2)}$ for the model BVP (25) given in Table 3: excitation frequency $\omega\varepsilon = 2$.

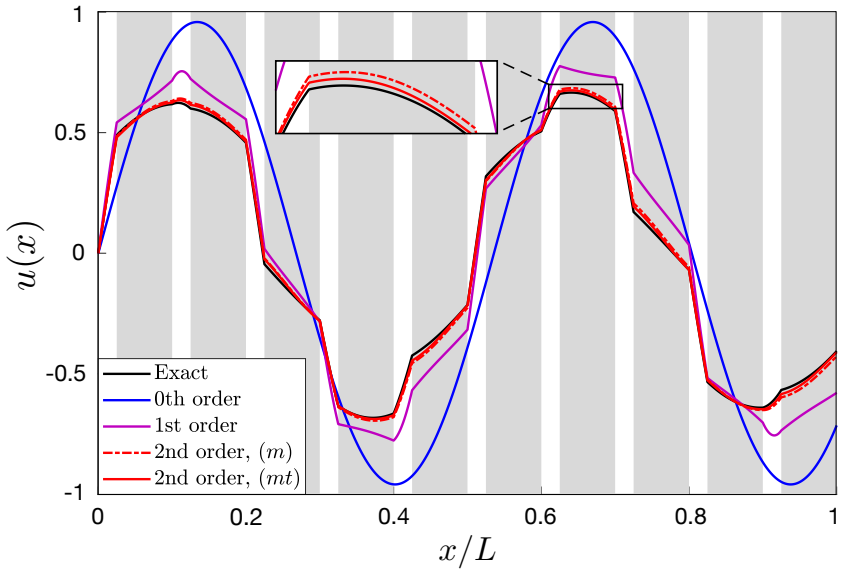

Figure 8: Exact wave motion u versus homogenized approximations $\tilde{u}^{(0)}$, $\tilde{u}^{(1)}$ and $\tilde{u}^{(2)}$ for the model BVP (25) given in Table 3: excitation frequency $\omega\varepsilon = 2$.

4.3. Homogenized transmission problem

This section investigates the homogenized approximation of a *transmission problem* for bilaminate rod $Y_L = (0, L)$ that is bonded, at its terminal sections, to homogeneous pieces $Y^- = (-L, 0)$ and $Y^+ = (L, 2L)$ endowed with respective material properties (E_-, ρ_-) and (E_+, ρ_+). The Dirichlet boundary conditions are applied at $x = -L$ and $x = 2L$. In this case, the displacement field u satisfies the BVP

$$\begin{aligned} &E_\pm u_{,xx} + \rho_\pm \omega^2 u = 0 \quad \text{for } x \in Y^\pm, \\ &(Eu_{,x})_{,x} + \rho\omega^2 u = 0 \quad \text{for } x \in Y_L, \\ &u = 0 \qquad\qquad\qquad\quad \text{at } x = -L, \\ &u = u_L \qquad\qquad\qquad\quad \text{at } x = 2L, \end{aligned} \tag{61}$$

that includes the continuity conditions

$$x = 0 \ : \begin{cases} u(0^-) = u(0^+) \\ (E_- u_{,x})(0^-) = (Eu_{,x})(0^+) \end{cases}, \qquad x = L \ : \begin{cases} u(L^-) = u(L^+) \\ (Eu_{,x})(L^-) = (E_+ u_{,x})(L^+) \end{cases}. \tag{62}$$

The exact solution of this problem is provided in Appendix B. Following the study of the model BVP in Section 4.2, we consider the approximations $U^{(0)}, \tilde{u}^{(1)}$ and $\tilde{u}^{(2)}$ according to (60) over the full domain

$$Y^- \cup \overline{Y_L} \cup Y^+. \tag{63}$$

The problems satisfied by the mean fields $U^{(0)}, U^{(1)}$ and $U^{(2)}$ (supported in the full domain) are constructed following the discussion in Section 3.5, as specified in Appendix B (see problems (B.6-B.7), (B.9-B.10) and (B.12-B.13), respectively). The expressions for the cell functions P_1 and P_2 (supported in Y_L only) are provided in Appendix A.

The sought approximations are compared in Fig. 9 with the exact field u, at $\omega\varepsilon = 2.5$ (the middle grey square in Fig. 1), for the problem parameters listed in Table 4. As can be seen from the display, a good agreement is obtained only by the second-order approximation $\tilde{u}^{(2)}$, especially when using the (mt) variant of the governing field equation. We further note that the lack of fit inside the periodic inclusion (however small or large) is in fact amplified in the right homogeneous piece, Y^+.

The behavior as $\varepsilon \to 0$ of the affiliated approximation errors

$$\frac{\|u - \tilde{u}^{(j)}\|_n}{\|u\|_n}, \qquad j = 0, 1, 2, \quad n = 0, 1,$$

this time computed over the full domain (63), is plotted in Fig. 10 (we keep $\omega = 2\pi$ and let $N \to +\infty$). As predicted, we observe *the same* respective orders of convergence as for the model BVP in Fig. 5. In this case, however, the optimal (mt) model is seen to improve the approximation over the reference (m) model more significantly than before.

ω	L	ε	α	γ_E	γ_ρ	(E_1, ρ_1)	(E_-, ρ_-)	(E_+, ρ_+)	u_L
2π	$50/(4\pi)$	$5/(4\pi)$	$1/4$	6	$3/2$	$(1, 2/3)$	$(\gamma_E E_1, \gamma_\rho \rho_1)$	(E_1, ρ_1)	1

Table 4: Parameters of the transmission problem (61)–(62) used in numerical simulations: $\omega\varepsilon = 2.5$.

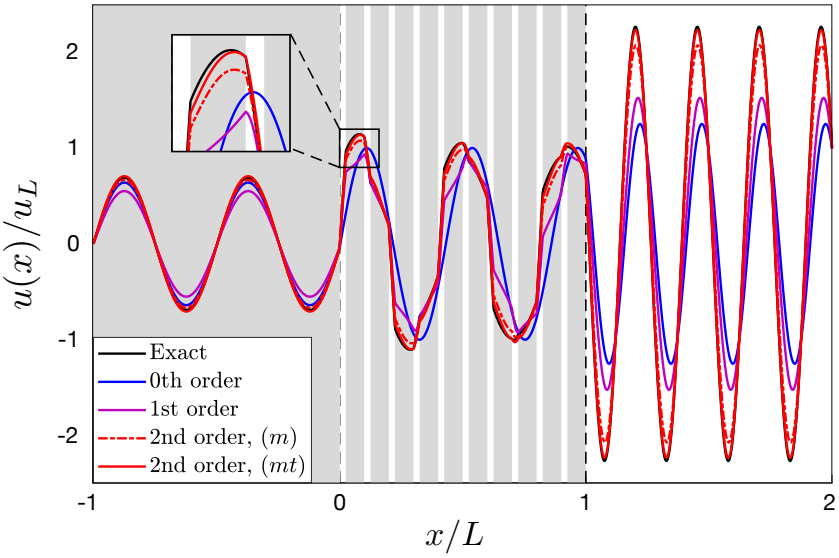

Figure 9: Exact wave motion u versus homogenized approximations $\tilde{u}^{(0)}$, $\tilde{u}^{(1)}$ and $\tilde{u}^{(2)}$ for the transmission problem (61) given in Table 4: excitation frequency $\omega\varepsilon = 2.5$. The shaded regions indicate lamina within the rod where $E = \gamma_E E_1$ and $\rho = \gamma_\rho \rho_1$.

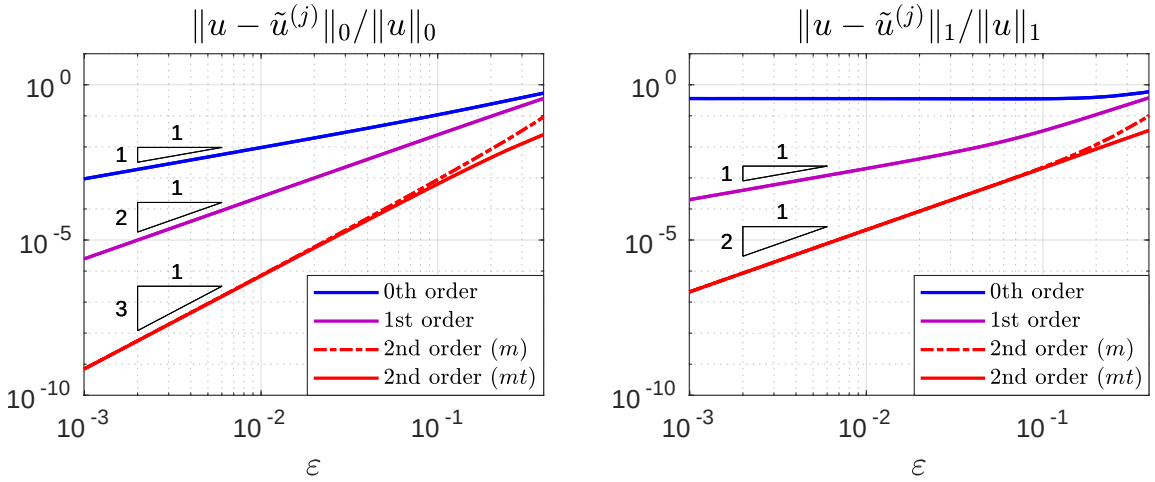

Figure 10: Relative L^2 and H^1 errors of the homogenized approximations $\tilde{u}^{(j)}$ $(j = 0, 1, 2)$ versus ε for the transmission problem (61) given in Table 4.

5. Summary and outlook

The main contribution of this paper resides in the development and asymptotic analysis of effective boundary and transmission conditions governing the first- and second-order mean field approximations of 1D waves in periodic media. The homogenization ansatz is established, up to the second order of expansion, for both types of problems, exposing the effective boundary (and transmission) conditions as those of Robin type. Rigorous asymptotic analysis is performed for boundary conditions, while the applicability to transmission conditions is demonstrated via numerical experiments. As a side result, an optimized second-order model of the homogenized field equation is proposed for 1D periodic media, that approximates more accurately the germane dispersion relationship and generally enhances the performance of second-order approximation. The proposed homogenization framework is applied toward the long-wavelength approximation of wave motion in finite periodic bilaminates, subject to both boundary and transmission conditions. The results of numerical simulations that include dispersion diagrams, mean-field approximations, "full"-field approximations, and convergence studies are found to consistently support the mathematical analysis. The developments in this study lay the groundwork for several future studies, including (i) analysis of the effective boundary and transmission conditions

for the (xmt) homogenized field equation that features an $O(\varepsilon^2)$ singular perturbation; (ii) homogenization of the corresponding time-domain problems; (iii) extensions to finite-frequency, finite-wavenumber problems motivated by the recent homogenization analyses of the wave equation Craster et al. (2010); Guzina et al. (2019); and (iv) effective boundary and transmission conditions for 1D eigenvalue problems Moskow and Vogelius (1997); Cornaggia (2016).

Appendix A. Cell functions and cell stresses for periodic bilaminate

This section provides closed-form expressions, in our notation, for the first two cell functions (P_1, P_2) and first two cell stresses (Σ_1, Σ_2) assuming periodic bilaminate (46) with the unit cell $Y = (0, 1)$. Similar cell functions can be found in Andrianov et al. (2008) with the unit cell taken as $(-1/2, 1/2)$ instead.

First cell problem:. The first cell function P_1 solving (9) is given by

$$P_1(y) \;=\; \begin{cases} (n_E-1)\Big(y-\dfrac{\alpha}{2}\Big), & y\in[0,\alpha],\\[2mm] -(n_E-1)\dfrac{\alpha}{1-\alpha}\Big(y-\dfrac{1+\alpha}{2}\Big), & y\in[\alpha,1]. \end{cases} \tag{A.1}$$

The affiliated cell stress is constant, namely $\Sigma_0(y) = (\hat{E}(y)/\mathcal{E}_0)(1 + P_{1,y})(y) = 1$.

Second cell problem:. The second cell function P_2 solving (10) can be computed as

$$P_2(y) \;=\; \begin{cases} P_2(0) + A_1 y(y-\alpha), & y\in[0,\alpha],\\ P_2(0) + A_2\left[y(y-(1+\alpha))+\alpha\right], & y\in[\alpha,1], \end{cases} \tag{A.2}$$

where

$$P_2(0) \;=\; \frac{\alpha^2}{12}\Big[\frac{n_E}{n_\rho} + \frac{1-3\alpha}{\alpha}n_E - \frac{1-\alpha}{\alpha n_\rho} + 1\Big] \tag{A.3}$$

and

$$A_1 \;=\; \frac{1}{2}\Big[\frac{n_E}{n_\rho} - 2n_E + 1\Big], \qquad A_2 \;=\; \frac{1}{2}\Big(\frac{\alpha}{1-\alpha}\Big)^2\Big[\frac{n_E}{n_\rho} + \frac{1-2\alpha}{\alpha}n_E - \frac{1}{\alpha n_\rho} + 1\Big]. \tag{A.4}$$

On the basis of (22) and (A.2)–(A.4), we further find that

$$\Sigma_1(y) \;=\; \begin{cases} -\Big(1-\dfrac{1}{n_\rho}\Big)\Big(y-\dfrac{\alpha}{2}\Big), & y\in[0,\alpha],\\[2mm] \Big(1-\dfrac{1}{n_\rho}\Big)\Big(\dfrac{\alpha}{1-\alpha}\Big)\Big(y-\dfrac{1+\alpha}{2}\Big), & y\in[\alpha,1]. \end{cases} \tag{A.5}$$

Third cell problem:. By virtue of (11) and (22), second cell stress Σ_2 satisfies

$$\Sigma_{2,y} \;=\; \frac{\hat{\rho}}{\varrho_0}P_1 - \Sigma_1 \quad\text{and}\quad \mathcal{E}_0\Sigma_2 \;=\; \hat{E}(P_2 + P_{3,y}) \qquad \text{for } x\in Y, \tag{A.6}$$

along with continuity requirements at the interfaces. Integrating the first of (A.6), one finds

$$\Sigma_2(y) \;=\; \begin{cases} \Sigma_2(0) + B_1 y(y-\alpha), & y\in[0,\alpha],\\ \Sigma_2(0) + B_2\left[y(y-(1+\alpha))+\alpha\right], & y\in[\alpha,1], \end{cases}$$

where

$$B_1 \;=\; \frac{1}{2}\Big[\frac{n_E}{n_\rho} - \frac{2}{n_\rho} + 1\Big], \qquad B_2 \;=\; \frac{1}{2}\Big(\frac{\alpha}{1-\alpha}\Big)^2\Big[\frac{n_E}{n_\rho} + \frac{1-2\alpha}{\alpha n_\rho} - \frac{n_E}{\alpha} + 1\Big].$$

Using the second of (A.6) and identity $0 = \langle P_{3,y}\rangle = \langle \mathcal{E}_0\Sigma_2/\hat{E} - P_2\rangle = \langle \mathcal{E}_0\Sigma_2/\hat{E}\rangle$, we find

$$\Sigma_2(0) \;=\; \frac{n_E}{6}\Big[\alpha^3 B_1 + \frac{(1-\alpha)^3}{\gamma_E}B_2\Big]. \tag{A.7}$$

As an illustration, the first two cell functions (P_1, P_2) and cell stresses (Σ_1, Σ_2) corresponding to bilaminate (59) are plotted in Fig. A.11.

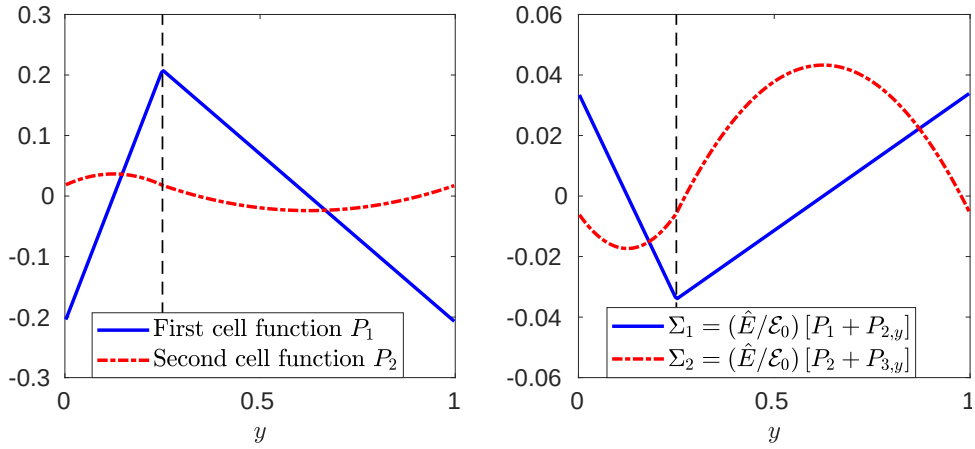

Figure A.11: Cell functions (P_1, P_2) and cell stresses (Σ_1, Σ_2) for $\alpha = 0.25$, $\gamma_E = 6$ and $\gamma_\rho = 1.5$.

Appendix B. Exact solution and homogenized models of the transmission problem for periodic bilaminate

This section provides: (i) exact solution of the transmission problem (61); (ii) the zeroth-, first- and second-order homogenized problems governing the mean fields, and (iii) their respective solutions.

Appendix B.1. Exact solution

In the homogeneous pieces $Y^\pm$ surrounding the inclusion, the displacement field u can be written as

$$u(x) \;=\; \begin{cases} U^-(x+L), & x \in [-L, 0], \\ U^+(x-L), & x \in [L, 2L], \end{cases} \tag{B.1}$$

where

$$U^\pm(x) \;=\; A^\pm \cos(k_\pm x) \;+\; B^\pm \sin(k_\pm x)$$

and

$$k_\pm = \frac{\omega}{c_\pm}, \qquad \text{and} \quad c_\pm = \sqrt{\frac{E_\pm}{\rho_\pm}}.$$

As a result, the boundary conditions $u(-L) = 0$ and $u(2L) = u_L$ reduce to

$$A^- \;=\; 0 \quad \text{and} \quad A^+ \cos(k_+ L) + B^+ \sin(k_+ L) \;=\; u_L. \tag{B.2}$$

In the periodic inclusion, E and ρ in (61) are piecewise-constant according to (46). With $N = L/\varepsilon$ being the number of cells comprising the inclusion, we denote by $x_n = n\varepsilon$ $(n = \overline{0, N})$ the positions of cell boundaries, and we let

$$k_1 = \frac{\omega}{c_1}, \qquad k_2 = k_1 \sqrt{\frac{\gamma_\rho}{\gamma_E}}$$

be the wavenumbers in the two lamina. Then, for $x \in (x_n, x_{n+1})$, $n = \overline{0, N-1}$, $u(x)$ can be written in terms of the coefficients $a_n^{(1)}, b_n^{(1)}, a_n^{(2)}$ and $b_n^{(2)}$ as

$$u(x) = \begin{cases} a_n^{(1)} \cos\left(k_1 (x - x_n)\right) + b_n^{(1)} \sin\left(k_1 (x - x_n)\right), & x \in [x_n, x_n + \alpha\varepsilon], \\ a_n^{(2)} \cos\left(k_2 (x - x_n - \alpha\varepsilon)\right) + b_n^{(2)} \sin\left(k_2 (x - x_n - \alpha\varepsilon)\right), & x \in [x_n + \alpha\varepsilon, x_{n+1}]. \end{cases} \tag{B.3}$$

Letting

$$\boldsymbol{M}(x) = \begin{bmatrix} \cos(x) & \sin(x) \\ -\sin(x) & \cos(x) \end{bmatrix}, \qquad \boldsymbol{T}(\eta) = \begin{bmatrix} 1 & 0 \\ 0 & \eta \end{bmatrix},$$

we next write (i) the transmission conditions at $x = 0$ and at $x = L$, and (ii) the transmission conditions for each interface within the microstructure as

$$\begin{aligned}
x = 0: \quad & \begin{bmatrix} a_0^{(1)} \\ b_0^{(1)} \end{bmatrix} = \boldsymbol{T}\Big(\frac{\sqrt{E_-\rho_-}}{\sqrt{E_1\rho_1}}\Big) \cdot \boldsymbol{M}(k_- L) \cdot \begin{bmatrix} A^- \\ B^- \end{bmatrix}, \\
x = x_n + \alpha\varepsilon: \quad & \begin{bmatrix} a_n^{(2)} \\ b_n^{(2)} \end{bmatrix} = \boldsymbol{T}\Big(\frac{1}{\sqrt{\gamma_E\gamma_\rho}}\Big) \cdot \boldsymbol{M}(k_1\alpha\varepsilon) \begin{bmatrix} a_n^{(1)} \\ b_n^{(1)} \end{bmatrix}, \\
x = x_{n+1}: \quad & \begin{bmatrix} a_{n+1}^{(1)} \\ b_{n+1}^{(1)} \end{bmatrix} = \boldsymbol{T}\Big(\sqrt{\gamma_E\gamma_\rho}\Big) \cdot \boldsymbol{M}(k_2(1-\alpha)\varepsilon) \cdot \begin{bmatrix} a_n^{(2)} \\ b_n^{(2)} \end{bmatrix}, \\
x = L: \quad & \begin{bmatrix} A^+ \\ B^+ \end{bmatrix} = \boldsymbol{T}\Big(\frac{\sqrt{E_1\rho_1}}{\sqrt{E_+\rho_+}}\Big) \cdot \begin{bmatrix} a_N^{(1)} \\ b_N^{(1)} \end{bmatrix},
\end{aligned} \tag{B.4}$$

where we used two auxiliary coefficients, $a_N^{(1)}$ and $b_N^{(1)}$ (corresponding to a "virtual" half-cell $[L, L+\alpha\varepsilon]$), to simplify the expressions. On defining the cell transfer matrix, $\boldsymbol{M}_\varepsilon$, as

$$\boldsymbol{M}_\varepsilon \;=\; \boldsymbol{T}\left(\sqrt{\gamma_E\gamma_\rho}\right) \cdot \boldsymbol{M}(k_2(1-\alpha)\varepsilon) \cdot \boldsymbol{T}\Big(\frac{1}{\sqrt{\gamma_E\gamma_\rho}}\Big) \cdot \boldsymbol{M}(k_1\alpha\varepsilon)$$

and combining equations (B.4), the second boundary condition in (B.2) becomes

$$\left(\boldsymbol{M}_{\text{tot}} \cdot \begin{bmatrix} 0 \\ B^- \end{bmatrix}\right) \cdot \begin{bmatrix} 1 \\ 0 \end{bmatrix} \;=\; u_L, \tag{B.5}$$

where the "total" transfer matrix is given by

$$\boldsymbol{M}_{\text{tot}} \;=\; \boldsymbol{M}(k_+ L) \cdot \boldsymbol{T}\Big(\frac{\sqrt{E_1\rho_1}}{\sqrt{E_+\rho_+}}\Big) \cdot \big[\boldsymbol{M}_\varepsilon\big]^N \cdot \boldsymbol{T}\Big(\frac{\sqrt{E_-\rho_-}}{\sqrt{E_1\rho_1}}\Big) \cdot \boldsymbol{M}(k_- L).$$

Note that the eigenvalues of transmission problem (61) correspond to frequencies ω for which (B.5) with $u_L = 0$ admits a non-trivial solution. On writing the characteristic function as

$$f_{\text{tot}}(\omega) \;=\; \begin{bmatrix} 1 \\ 0 \end{bmatrix}^{\mathsf{T}} \cdot \boldsymbol{M}_{\text{tot}} \cdot \begin{bmatrix} 0 \\ 1 \end{bmatrix}$$

and assuming $f_{\text{tot}}(\omega) \neq 0$, we consequently find from (B.5) that

$$B^- = \frac{u_L}{f_{\text{tot}}(\omega)}.$$

The coefficients $a_n^{(1)}, b_n^{(1)}, a_n^{(2)}$ and $b_n^{(2)}$ ($n = \overline{0, N-1}$), together with A^+ and B^+, are then computed from the transmission conditions (B.4), thus yielding the complete solution by way of (B.1) and (B.3).

Remark B.1. *For simplicity, we assumed the displacement boundary conditions at both ends of the composite rod in transmission problem (61). Nonetheless, considering other boundary conditions would result in a similar expression for the characteristic function f_{tot} and solution u. For instance assuming prescribed traction, $E_+ u_{,x}(2L) = \sigma_L$, at the "right" end, we obtain the characteristic function*

$$f_{\text{tot}}^{\text{tr}}(\omega) := \begin{bmatrix} 0 \\ 1 \end{bmatrix}^{T} \cdot \boldsymbol{M}_{\text{tot}} \cdot \begin{bmatrix} 0 \\ 1 \end{bmatrix}$$

so that, for $f_{\text{tot}}^{\text{tr}}(\omega) \neq 0$, we have

$$B_{\text{tr}}^- = \frac{\sigma_L}{E_+ \, k_+ \, f_{\text{tot}}^{\text{tr}}(\omega)}.$$

Appendix B.2. Homogenized models

We now apply the homogenization procedure to transmission problem (61). We pursue this goal by first writing the transmission conditions in terms of the *total fields*, and then applying these interfacial requirements to the mean fields so that the microscopic information is retained.

Zeroth-order model.. The leading-order homogenized field $U^{(0)} = U_0$ satisfies the field equations

$$\begin{aligned} U^{(0)}_{,xx} + k_\pm^2 U^{(0)} &= 0 \quad \text{for } x \in Y^\pm, \\ U^{(0)}_{,xx} + k_0^2\, U^{(0)} &= 0 \quad \text{for } x \in Y_L, \end{aligned} \tag{B.6}$$

together with the boundary and transmission conditions

$$U^{(0)}(-L) = 0, \quad \begin{cases} U^{(0)}(0^-) = U^{(0)}(0^+), \\ E_- U^{(0)}_{,x}(0^-) = \mathcal{E}_0 U^{(0)}_{,x}(0^+), \end{cases} \quad \begin{cases} U^{(0)}(L^-) = U^{(0)}(L^+), \\ \mathcal{E}_0 U^{(0)}_{,x}(L^-) = E_+ U^{(0)}_{,x}(L^+), \end{cases} \quad U^{(0)}(2L) = u_L. \tag{B.7}$$

We next let

$$U^{(0)}(x) \;=\; \begin{cases} U^-(x+L), & x \in [-L, 0], \\ a_0 \cos(k_0 x) + b_0 \sin(k_0 x), & x \in [0, L], \\ U^+(x-L), & x \in [L, 2L], \end{cases} \tag{B.8}$$

where U^- and U^+ are given by (B.1). On writing the boundary and transmission conditions (B.7) in terms of $A^\pm, B^\pm, a_0$ and b_0, we obtain the characteristic function

$$f_0(\omega) := \left[\begin{array}{c} 1 \\ 0 \end{array}\right]^{\mathtt{T}} \cdot \boldsymbol{M}^+ \cdot \boldsymbol{T}_0^+ \cdot \boldsymbol{M}_0 \cdot (\boldsymbol{T}_0^-)^{-1} \cdot \boldsymbol{M}^- \cdot \left[\begin{array}{c} 0 \\ 1 \end{array}\right],$$

where

$$\boldsymbol{M}^\pm = \boldsymbol{M}(k_\pm L), \qquad \boldsymbol{M}_0 = \boldsymbol{M}(k_0 L), \qquad \boldsymbol{T}_0^\pm = \boldsymbol{T}\Big(\frac{\sqrt{\mathcal{E}_0 \varrho_0}}{\sqrt{E_\pm \rho_\pm}}\Big).$$

When $f_0(\omega) \neq 0$, the transmission problem (B.6)–(B.7) is well-posed, and its solution is given by

$$B^- = \frac{u_L}{f_0(\omega)}.$$

First-order model.. The first-order total mean field $U^{(1)}$ satisfies the field equations

$$\begin{aligned} U^{(1)}_{,xx} + k_\pm^2 U^{(1)} &= 0 \quad \text{for } x \in Y^\pm, \\ U^{(1)}_{,xx} + k_0^2\, U^{(1)} &= 0 \quad \text{for } x \in Y_L, \end{aligned} \tag{B.9}$$

along with the usual boundary conditions ($U^{(1)}(-L) = 0$ and $U^{(1)}(2L) = u_L$) and the enhanced transmission conditions

$$\begin{cases} U^{(1)}(0^-) = \big[U^{(1)} + \varepsilon P_1(0) U^{(1)}_{,x}\big](0^+), \\ U^{(1)}_{,x}(0^-) = \dfrac{\mathcal{E}_0}{E_-}\big[\Sigma_0 U^{(1)}_{,x} - k_0^2\, \varepsilon \Sigma_1(0) U^{(1)}\big](0^+), \end{cases} \quad \begin{cases} \big[U^{(1)} + \varepsilon P_1(0) U^{(1)}_{,x}\big](L^-) = U^{(1)}(L^+), \\ \dfrac{\mathcal{E}_0}{E_+}\big[\Sigma_0 U^{(1)}_{,x} - k_0^2\, \varepsilon \Sigma_1(0) U^{(1)}\big](L^-) = U^{(1)}_{,x}(L^+), \end{cases} \tag{B.10}$$

featuring the $O(\varepsilon)$ boundary correctors stemming from the first-order approximations (31). With reference to (B.8), we next decompose $U^{(1)}$ into U^-, U^+ and the "interior" solution $a_1 \cos(k_0 x) + b_1 \sin(k_0 x)$, which transforms (B.10) into

$$\begin{aligned} x = 0: \quad \boldsymbol{M}^- \cdot \left[\begin{array}{c} A^- \\ B^- \end{array}\right] &= \boldsymbol{T}_0^- \cdot \boldsymbol{M}^{(1)}(0) \cdot \left[\begin{array}{c} a_1 \\ b_1 \end{array}\right], \\ x = L: \quad \left[\begin{array}{c} A^+ \\ B^+ \end{array}\right] &= \boldsymbol{T}_0^+ \cdot \boldsymbol{M}^{(1)}(k_0 L) \cdot \left[\begin{array}{c} a_1 \\ b_1 \end{array}\right], \end{aligned}$$

with

$$\boldsymbol{M}^{(1)}(x) \;=\; \boldsymbol{M}(x) \;+\; k_0 \varepsilon \boldsymbol{P}_1(0) \cdot \boldsymbol{N}(x)$$

and

$$\boldsymbol{P}_1(y) = \left[\begin{array}{cc} P_1(y) & 0 \\ 0 & \Sigma_1(y) \end{array}\right], \qquad \boldsymbol{N}(x) = \left[\begin{array}{cc} -\sin(x) & \cos(x) \\ -\cos(x) & -\sin(x) \end{array}\right]. \tag{B.11}$$

The characteristic function is then given by

$$f_1(\omega) \;=\; \left[\begin{array}{c} 1 \\ 0 \end{array}\right]^{\mathtt{T}} \cdot \boldsymbol{M}^+ \cdot \boldsymbol{T}_0^+ \cdot \boldsymbol{M}^{(1)}(k_0 L) \cdot \big(\boldsymbol{M}^{(1)}(0)\big)^{-1} \cdot (\boldsymbol{T}_0^-)^{-1} \cdot \boldsymbol{M}^- \cdot \left[\begin{array}{c} 0 \\ 1 \end{array}\right],$$

so that ω is an eigenfrequency of the first-order problem if and only if $f_1(\omega) = 0$. When this is not the case, the solution of the transmission problem (B.9)–(B.10) is uniquely given by

$$B^- = \frac{u_L}{f_1(\omega)}.$$

Second-order model.. Assuming the (mt) model of the field equation examined in Section 3, the second-order mean field $U^{(2)}$ satisfies

$$\begin{aligned} &U^{(2)}_{,xx} + k_\pm^2 U^{(2)} = 0 \quad \text{for } x \in Y^\pm, \\ &U^{(2)}_{,xx} + k_{mt}^2 U^{(2)} = 0 \quad \text{for } x \in Y_L, \end{aligned} \tag{B.12}$$

where $k_{mt} = k_{mt}(\varepsilon)$ is given by (42). In this case the boundary conditions are $U^{(2)}(-L) = 0$ and $U^{(2)}(2L) = u_L$ as before, while the enhanced transmission conditions read

$$\begin{aligned} x = 0: &\begin{cases} U^{(2)}(0^-) = \big[\big(1 - k_{mt}^2\varepsilon^2 P_2(0)\big)\, U^{(2)} + \varepsilon P_1(0) U^{(2)}_{,x}\big](0^+), \\ U^{(2)}_{,x}(0^-) = \dfrac{\mathcal{E}_0}{E_-}\big[\big(\Sigma_0 - k_{mt}^2\varepsilon^2\Sigma_2(0)\big)\, U^{(2)}_{,x} - k_{mt}^2\varepsilon\Sigma_1(0) U^{(2)}\big](0^+), \end{cases} \\ x = L: &\begin{cases} \big[\big(1 - k_{mt}^2\varepsilon^2 P_2(0)\big)\, U^{(2)} + \varepsilon P_1(0) U^{(2)}_{,x}\big](L^-) = U^{(2)}(L^+), \\ \dfrac{\mathcal{E}_0}{E_+}\big[\big(\Sigma_0 - k_{mt}^2\varepsilon^2\Sigma_2(0)\big)\, U^{(2)}_{,x} - k_{mt}^2\varepsilon\Sigma_1(0) U^{(2)}\big](L^-) = U^{(2)}_{,x}(L^+), \end{cases} \end{aligned} \tag{B.13}$$

as driven by the second-order approximations (40). On decomposing $U^{(2)}$ into U^-, U^+ and the "interior" solution $a_2\cos(k_{mt}x) + b_2\sin(k_{mt}x)$, (B.13) become

$$\begin{aligned} x = 0: \quad \boldsymbol{M}^- \cdot \left[\begin{array}{c} A^- \\ B^- \end{array}\right] \;&=\; \boldsymbol{T}_{mt}^- \cdot \boldsymbol{M}^{(2)}(0) \cdot \left[\begin{array}{c} a_2 \\ b_2 \end{array}\right], \\ x = L: \qquad \left[\begin{array}{c} A^+ \\ B^+ \end{array}\right] \;&=\; \boldsymbol{T}_{mt}^+ \cdot \boldsymbol{M}^{(2)}(k_{mt}L) \cdot \left[\begin{array}{c} a_2 \\ b_2 \end{array}\right], \end{aligned}$$

where

$$\boldsymbol{T}_{mt}^\pm \;=\; \boldsymbol{T}\Big(\frac{\mathcal{E}_0 k_{mt}}{E_\pm k_\pm}\Big), \qquad \boldsymbol{M}^{(2)}(x) \;=\; \big(\boldsymbol{I} - k_{mt}^2\varepsilon^2\boldsymbol{P}_2(0)\big)\cdot\boldsymbol{M}(x) \;+\; k_{mt}\varepsilon\boldsymbol{P}_1(0)\cdot\boldsymbol{N}(x);$$

$\boldsymbol{P}_1$ and $\boldsymbol{N}$ are given by (B.11), and similarly $\boldsymbol{P}_2(y) = \mathrm{diag}(P_2(y), \Sigma_2(y))$. In this case, the characteristic function reads

$$f_2(\omega) \;=\; \left[\begin{array}{c} 1 \\ 0 \end{array}\right]^{\mathtt{T}} \cdot \boldsymbol{M}^+ \cdot \boldsymbol{T}_{mt}^+ \cdot \boldsymbol{M}^{(2)}(k_{mt}L) \cdot \big(\boldsymbol{M}^{(2)}(0)\big)^{-1} \cdot (\boldsymbol{T}_{mt}^-)^{-1} \cdot \boldsymbol{M}^- \cdot \left[\begin{array}{c} 0 \\ 1 \end{array}\right],$$

so that ω is an eigenfrequency of the second-order homogenized problem if and only if $f_2(\omega) = 0$. Assuming this is not the case, the solution of (B.12)–(B.13) is given by

$$B^- = \frac{u_L}{f_2(\omega)}.$$

References

Allaire, G. and Amar, M. (1999). Boundary layer tails in periodic homogenization. *ESAIM: Control, Optimisation and Calculus of Variations*, 4:209–243.

Allaire, G., Briane, M., and Vanninathan, M. (2016). A comparison between two-scale asymptotic expansions and Bloch wave expansions for the homogenization of periodic structures. *SeMA Journal*, 73(3):237–259.

Andrianov, I. V., Bolshakov, V. I., Danishevs'kyy, V. V., and Weichert, D. (2008). Higher order asymptotic homogenization and wave propagation in periodic composite materials. *Proceedings of the Royal Society of London A: Mathematical, Physical and Engineering Sciences*, 464(2093):1181–1201.

Armstrong, S., Kuusi, T., Mourrat, J.-C., and Prange, C. (2017). Quantitative analysis of boundary layers in periodic homogenization. *Archive for Rational Mechanics and Analysis*, 226(2):695–741.

Askes, H., Metrikine, A., Pichugin, A., and Bennett, T. (2008). Four simplified gradient elasticity models for the simulation of dispersive wave propagation. *Philosophical Magazine*, 88(28-29):3415–3443.

Bensoussan, A., Lions, J. L., and Papanicolau, G. (1978). *Asymptotic Analysis for Periodic Structures*. North-Holland, Amsterdam.

Brezis, H. (2011). *Functional Analysis, Sobolev Spaces and Partial Differential Equations*. Number 1 in 0172-5939. Springer-Verlag New York.

Cakoni, F., Guzina, B. B., and Moskow, S. (2016). On the homogenization of a scalar scattering problem for highly oscillating anisotropic media. *SIAM Journal on Mathematical Analysis*, 48(4):2532–2560.

Cakoni, F., Guzina, B. B., Moskow, S., and Pangburn, T. (2019). Scattering by a bounded highly oscillating periodic medium and the effect of boundary correctors. *SIAM Journal on Applied Mathematics*, 79(4):1448–1474.

Cioranescu, D. and Donato, P. (1999). *An introduction to homogenization*, volume 17 of *Oxford Lecture Series in Mathematics and its Applications*. Oxford University Press.

Claeys, X. and Delourme, B. (2013). High order asymptotics for wave propagation across thin periodic interfaces. *Asymptotic Analysis*, 83:35–82.

Cornaggia, R. (2016). *Development and use of higher-order asymptotics to solve inverse scattering problems*. Ph. D. thesis, ENSTA, Université Paris Saclay and CEGE, University of Minnesota.

Craster, R. V., Kaplunov, J., and Pichugin, A. V. (2010). High-frequency homogenization for periodic media. *Proceedings of the Royal Society A*, 466:2341–2362.

Dontsov, E. V., Tokmashev, R. D., and Guzina, B. B. (2013). A physical perspective of the length scales in gradient elasticity through the prism of wave dispersion. *International Journal of Solids and Structures*, 50(22-23):3674 – 3684.

Dumontet, H. (1986). Study of a boundary layer problem in elastic composite materials. *ESAIM: Mathematical Modelling and Numerical Analysis - Modélisation Mathématique et Analyse Numérique*, 20(2):265–286.

Fish, J., Chen, W., and Nagai, G. (2002). Non-local dispersive model for wave propagation in heterogeneous media: one-dimensional case. *International Journal for Numerical Methods in Engineering*, 54(3):331–346.

Gérard-Varet, D. and Masmoudi, N. (2012). Homogenization and boundary layers. *Acta Mathematica*, 209(1):133–178.

Guzina, B. B., Meng, S., and Oudghiri-Idrissi, O. (2019). A rational framework for dynamic homogenization at finite wavelengths and frequencies. *Proceedings of the Royal Society A*, 475:20180547.

Kaplunov, J. and Pichugin, A. (2009). On rational boundary conditions for higher-order long-wave models. In Borodich, F., editor, *IUTAM Symposium on Scaling in Solid Mechanics*, volume 10 of *Iutam Bookseries*, pages 81–90. Springer Netherlands.

Lamacz, A. (2011). Dispersive effective models for waves in heterogeneous media. *Mathematical Models and Methods in Applied Sciences*, 21(09):1871–1899.

Lin, Y.-H. and Meng, S. (2019). Leading and second order homogenization of an elastic scattering problem for highly oscillating anisotropic medium. *Journal of Elasticity*.

Marigo, J.-J. and Maurel, A. (2017). Second order homogenization of subwavelength stratified media including finite size effect. *SIAM Journal on Applied Mathematics*, 77(2):721–743.

Marigo, J.-J., Maurel, A., Pham, K., and Sbitti, A. (2017). Effective dynamic properties of a row of elastic inclusions: The case of scalar shear waves. *Journal of Elasticity*, 128(2):265–289.

Maurel, A. and Marigo, J.-J. (2018). Sensitivity of a dielectric layered structure on a scale below the periodicity: A fully local homogenized model. *Physical Review B*, 98(2).

McLean, W. (2000). *Strongly Elliptic Systems and Boundary Integral Equations*. Cambridge University Press.

Moskow, S. and Vogelius, M. (1997). First-order corrections to the homogenised eigenvalues of a periodic composite medium. a convergence proof. *Proceedings of the Royal Society of Edinburgh: Section A Mathematics*, 127:1263–1299.

Pichugin, A., Askes, H., and Tyas, A. (2008). Asymptotic equivalence of homogenisation procedures and fine-tuning of continuum theories. *Journal of Sound and Vibration*, 313(3-5):858 – 874.

Santosa, F. and Symes, W. W. (1991). A dispersive effective medium for wave propagation in periodic composites. *SIAM Journal on Applied Mathematics*, 51(4):984–1005.

Santosa, F. and Vogelius, M. (1993). First-order corrections to the homogenized eigenvalues of a periodic composite medium. *SIAM Journal on Applied Mathematics*, 53(6):1636–1668.

Semin, A., Delourme, B., and Schmidt, K. (2018). On the homogenization of the Helmholtz problem with thin perforated walls of finite length. *ESAIM: Mathematical Modelling and Numerical Analysis*, 52(1):29–67.

Vinoles, V. (2016). *Interface problems with metamaterials : modelling, analysis and simulations*. Ph. D. thesis, ENSTA, Université Paris-Saclay.

Wautier, A. and Guzina, B. B. (2015). On the second-order homogenization of wave motion in periodic media and the sound of a chessboard. *Journal of the Mechanics and Physics of Solids*, 78:382 – 414.